Theoretical and Applied Fracture Mechanics 127 (2023) 104091

Contents lists available at ScienceDirect

Theoretical and Applied Fracture Mechanics

journal homepage: www.elsevier.com/locate/tafmec

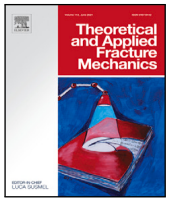

Direct evaluation of stress intensity factors and T-stress for bimaterial interface cracks using the extended isogeometric boundary element method

H.C. Andrade [a], J. Trevelyan [b], E.D. Leonel [a,*]

[a] Department of Structural Engineering, São Carlos School of Engineering, University of São Paulo, Av. Trabalhador São Carlense, 400, 13566-590, São Carlos SP, Brazil

[b] Department of Engineering, Durham University, South Road, Durham DH1 3LE, UK

ARTICLE INFO

Keywords:
Extended isogeometric boundary element method
Direct methods
Enriched formulations
Interface crack
Stress intensity factors
T-stress

ABSTRACT

This paper presents a new extended isogeometric boundary element method (XIGABEM) for the analysis of cracks in two-dimensional bimaterial interfaces. The classical NURBS approximations used in isogeometric formulations are augmented with functions based on the first two terms of the crack-tip stress and displacement series expansions. The first term is related to the complex stress intensity factor (SIF) and allows the numerical method to capture the singular and oscillatory near-tip behaviour, while the second accounts for the T-stress contribution to the solutions. The proposed enrichment strategy only introduces three additional degrees of freedom per crack tip, which are accommodated in a square linear system by a crack tip tying constraint and a novel condition on the stress parallel to the tip. These supplementary relations also cause the enrichment parameters to become proxies for the SIFs and T-stress. Therefore, the crack-tip factors can be obtained *directly* from the solution vector given by XIGABEM, eliminating the need for costly computational post-processing techniques. Several benchmark examples, including both straight and curved cracks, are presented to demonstrate the accuracy and convergence of the proposed method. The direct XIGABEM solutions for the SIFs and T-stress compare favourably against those from the literature.

1. Introduction

Applications of composite materials have received increasing interest in several industries over the past years. Due to their practical importance, the verification of structural integrity in these types of materials involves the investigation of fracture and delamination processes that occur at the interface between dissimilar media. Considering linear elastic fracture mechanics, early studies on interface cracks revealed that the stress and displacement fields near the crack tip exhibit an oscillatory behaviour [1–4]. As a result of this oscillatory nature, a zone of interpenetration has been demonstrated in regions close to the tip. According to Banks-Sills [5], this anomalous, non-physical behaviour was responsible for a hiatus of more than a decade in research on the subject. However, since the size of the contact zone in practical applications is small in comparison to the crack length [6], many studies were later conducted that included the oscillatory characteristic of the near-tip fields [7–10].

Due to the difficulties arising when working with singular and oscillatory fields, investigations of interface cracks are commonly based on the determination of crack tip parameters, especially the Stress Intensity Factors (SIFs) and the T-stress. The complex SIF defined by Rice [8] is able to represent the asymptotic singular stress field near the tip, and is a key parameter for delamination analyses. On the other hand, the T-stress is the first non-singular term in the eigenfunction expansion of the stress field and provides relevant aspects for fracture analysis [11], such as assessment of stability [12], kinked cracks [13,14] and definition of the plastic zone near the tip [15].

Closed-form solutions for the SIFs and T-stress of interface cracks are available only for a limited number of configurations [16–18] and solutions for the vast majority of industrially relevant applications can be determined only by numerical methods, such as the Finite Element Method (FEM) [19–21] and the Boundary Element Method (BEM) [22–25]. One of the variants of FEM, the eXtended FEM (XFEM), is perhaps the most popular method for the analysis of interface cracks and extraction of tip parameters [26–29]. The XFEM is derived by enriching the FE approximation space through partition of unity enrichment [30,31] with functions defined from the analytical expansion of the near-tip fields. The BEM is another widely applied numerical method which is particularly suitable for crack analysis due to its boundary-only discretisation and accurate representation of the internal fields. Early BEM strategies for the analysis of interface cracks consisted

* Corresponding author.
E-mail addresses: heider.andrade@alumni.usp.br (H.C. Andrade), jon.trevelyan@durham.ac.uk (J. Trevelyan), edleonel@sc.usp.br (E.D. Leonel).

https://doi.org/10.1016/j.tafmec.2023.104091
Received 19 April 2023; Received in revised form 6 August 2023; Accepted 13 September 2023
Available online 20 September 2023

Nomenclature

A

a	Half crack length
c_{ij}	Jump term
d_j	Displacement control parameters
E	Young's modulus
J	Jacobian of the transformation
K_1, K_2	Modes 1 and 2 SIFs
K_T	T-stress parameter
n	Number of control points
n_j	Normal vector components
p	Order of the NURBS
p_j	Traction components
$R_{i,p}$	NURBS functions
T	T-stress
T_{jk}	Rotation matrix
t_j	Traction control parameters
U^*_{ij}, P^*_{ij}	Fundamental solutions
u_j	Displacement components
w_i	NURBS weights

B

δ_{ij}	Kronecker delta
Δ^n_j and Θ^n_j	Displacement functions
Γ	Boundary
$\hat{\xi}$	Parent space coordinate
κ	Kolosov constant
Λ	Weight vector
μ	Shear modulus
ν	Poisson's ratio
Ω	Domain
ϕ	Shape functions
ψ_{kM}	Displacement enrichment functions (1st term)
ρ, θ	Crack-tip polar coordinates
σ_{ij}	Stress components
$\Sigma^n_{ij}, \Upsilon^n_{ij}$	Stress functions
ε	Oscillatory parameter
φ	Displacement enrichment functions (2nd term)
ϖ_{kM}	Traction enrichment functions (2nd term)
Ξ	Knot vector
ξ	Parametric coordinate

C

BEM	Boundary element method
BIE	Boundary integral equation
EFG	Element-free Galerkin
FEM	Finite element method
NURBS	Non-uniform rational B-spline
SBFEM	Scaled boundary finite element method
SIF	Stress intensity factor
XBEM	Extended boundary element method
XFEM	Extended finite element method
XIGABEM	Extended isogeometric boundary element method
xSBFEM	Extended scaled boundary finite element method

S

λ	Crack tip
B	External boundary
C	Crack
e	Element
I	Interface
M	SIF mode
m	Local index (element)
s	Material

Z

$\Im$	Imaginary part operator
$\mathbf{d}, \mathbf{t}, \mathbf{y}, \mathbf{K}, \mathbf{f}$	BEM sub-vectors
$\mathbf{H}, \mathbf{G}, \mathbf{A}$	BEM sub-matrices
i	Imaginary unit $\left(=\sqrt{-1}\right)$
$\Re_n$	N-th crack parameter
$\Re$	Real part operator

mainly in coupling the multi-region technique with a quarter-point element formulation [32–34]. This special crack-tip element was originally developed for cracks in homogeneous materials and is able to represent the square root singularity in the analytical near-tip solutions. However, the oscillatory behaviour over interface cracks is not included in the quarter-point formulation, so such a strategy leads to the improper representation of the near-tip fields, and this is particularly evident when large differences between the materials along the interface are considered. Recently, Gu and Zhang [35] proposed a new crack-tip element able to represent the analytical near-tip solution for interface cracks and were able to compute the SIFs using the displacement extrapolation technique. However, the use of special tip elements restricts the analytical behaviour to crack-tip elements, while more accuracy can be realised by considering more elements to be within the local influence of the crack-tip singularity. Besides, the optimum choice for the size of the special elements is not clear [36–39].

Several methods have been proposed for extracting the SIFs and T-stress of interface cracks, and they have been mainly based on the interaction integral (or M-integral). This approach is an extension of the path-independent J-integral [40] and relies on the existence of auxiliary fields for evaluating the crack parameters. While the definition of auxiliary fields is straightforward for straight cracks, this task is cumbersome when dealing with curvilinear cracks since the omission of the curvature effect in the definition of the auxiliary fields may degrade the accuracy and convergence of the interaction integral method [41,42]. To overcome this drawback, some XFEM approaches have been proposed to compute the crack parameters *directly* from the solution of the system of equations without extra post-processing [43,44]. These so-called *direct* methods have also been applied for SIF and T-stress extraction in interface cracks in the Scaled Boundary Finite Element Method (SBFEM) framework [45,46].

Over the past decade, enriched BEM formulations have been developed to improve the near-tip solution in fracture analysis of homogeneous materials, giving rise to the eXtended BEM (XBEM) [47–50]. An eXtended IsoGeometric Analysis BEM (XIGABEM) has also been proposed to take advantage of the use of both Non-Uniform Rational B-Splines (NURBS) and enrichment functions in the numerical analyses [51,52]. NURBS are the standard mathematical model used for describing curves and surfaces in computer-aided design software and provide an accurate geometry description; one, indeed, that is exact for conic sections. The fact that both the NURBS approximation and the BEM deal with quantities entirely on the boundary makes the coupling between them natural, which promotes significant effort savings during

the meshing process for the numerical model. Nevertheless, like the Lagrange polynomials used in conventional BEM, the NURBS basis functions fail to describe the analytical mechanical fields near the crack tip. Hence, the enrichment of the approximation space in the XIGABEM framework creates an approach that, in addition to the accurate geometry description, is also able to capture the singular near-tip behaviour.

The introduction of enrichment degrees of freedom in the XBEM and XIGABEM formulations requires the definition of an equal number of auxiliary equations in order to achieve a square linear system. As demonstrated by many previous works [48–50,52], the use of a crack tip tying constraint to accommodate the additional enrichment parameters allows these parameters to become proxies for the SIFs. Therefore, these crack parameters can be obtained *directly* from the solution vector given by the method. Consequently, we call this approach a *direct* method, and it therefore provides significant benefits by precluding the need for post-processing by techniques such as the interaction integral. This is particularly beneficial in the BEM context since it saves the computational cost of evaluating the mechanical fields at several internal points. As a result, a substantial reduction in execution time can be achieved when using the direct method without prejudice to the accuracy of the solutions [52]. Note that the use of the term *direct* is not to be confused with the classical direct and indirect boundary element methods.

All the aforementioned enriched BEM works are concerned only with homogeneous materials. Furthermore, no direct evaluation of the T-stress using the extended BEM approach has yet been reported in the literature.

In this context, this paper presents a novel XIGABEM formulation for the analysis of bimaterial interface cracks in 2D domains. It is the first extended BEM scheme developed for interface cracks, and the first also to extend the enrichment to the direct T-stress calculation by including the second term of the near-tip asymptotic expansion in the approximation space. The presence of singular traction fields to be recovered on interfaces at the crack tip requires the consideration for the first time of singular enrichment functions. In addition to the classical use of the crack tip tying constraint to accommodate the degrees of freedom related to the SIFs in the linear system, a novel constraint on the stress parallel to the interface at the crack tip is applied to determine the T-stress parameter. We demonstrate that the proposed direct XIGABEM formulation is able to recover accurate solutions for the crack parameters, including for curvilinear crack paths, without incurring costly computational post-processing techniques.

The remainder of this paper is organised as follows: Section 2 describes the fundamentals of interface fracture mechanics that form the basis for the novel XIGABEM formulation presented in Section 3. The accuracy and stability of the proposed approach are verified in six numerical benchmark examples presented in Section 4, while Section 5 draws some conclusions about the extended isogeometric formulation developed in this study.

2. Interface fracture mechanics

Let Ω be a 2D-domain consisting of two dissimilar isotropic and elastic materials. The material above the interface is denoted as material 1, while the material below is defined as material 2, as illustrated in Fig. 1. Consider a crack lying along the interface, with upper and lower crack surfaces represented by Γ_1^C and Γ_2^C, respectively. Moreover, assume that the interface boundary Γ_1^I from material 1 is perfectly bonded with the interface boundary Γ_2^I from material 2. In this situation, the complete expansion for the crack-tip stress field is given by [53]:

$$\sigma_{ij}(\rho,\theta,s) = \sum_{n=1}^{\infty} \frac{\rho^{\frac{n-2}{2}}}{\sqrt{2\pi}} \left\{ \Re\left[\aleph_n \rho^{\mathrm{i}\epsilon_n}\right] \Sigma_{ij}^n(\theta,s) + \Im\left[\aleph_n \rho^{\mathrm{i}\epsilon_n}\right] Y_{ij}^n(\theta,s) \right\}, \tag{1}$$

where $i,j = 1,2$ denote the direction in the crack-tip coordinate system (x_1,x_2), (ρ,θ) are the crack-tip polar coordinates shown in Fig. 1, $s = 1,2$

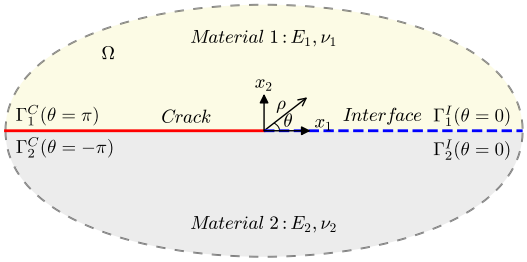

Fig. 1. Interface crack between two dissimilar materials.

indicates the material 1 and 2, respectively, $\aleph_n \in \mathbb{C}$ represents the nth crack parameter, and $\Sigma_{ij}^n(\theta,s)$ and $Y_{ij}^n(\theta,s)$ are the stress functions given in Appendix A. The symbols $\Re$ and $\Im$ denote, respectively, the real and imaginary parts of the quantity in brackets $[\bullet]$ and $\mathrm{i} = \sqrt{-1}$ is the imaginary unit. ϵ_n is defined as follows:

$$\epsilon_n = \begin{cases} \epsilon = \frac{1}{2\pi} \log \frac{\mu_2\kappa_1+\mu_1}{\mu_1\kappa_2+\mu_2}, & \text{if } n = 1,3,5,\ldots \\ 0, & \text{if } n = 2,4,6,\ldots, \end{cases} \tag{2}$$

where ϵ is known as the oscillatory parameter since it is related to the oscillatory behaviour of the odd terms in the solution. $\mu_s = E_s/\left[2(1+\nu_s)\right]$ is the shear modulus and κ_s is the Kolosov constant defined as $\kappa_s = 3-4\nu_s$ for plane strain and $\kappa_s = \left(3-\nu_s\right)/\left(1+\nu_s\right)$ for plane stress. E_s and ν_s represent, respectively, the Young's modulus and the Poisson's ratio of material $s = 1,2$.

The general form of the crack-tip displacement field is also provided by Deng [53], to be:

$$u_j(\rho,\theta,s) = \sum_{n=1}^{\infty} \frac{\rho^{n/2}}{\sqrt{2\pi}} \left\{ \Re\left[\aleph_n \rho^{\mathrm{i}\epsilon_n}\right] \Delta_j^n(\theta,s) + \Im\left[\aleph_n \rho^{\mathrm{i}\epsilon_n}\right] \Theta_j^n(\theta,s) \right\}, \tag{3}$$

where $\Delta_j^n(\theta,s)$ and $\Theta_j^n(\theta,s)$ are the displacement functions given in Appendix A.

In this study, we are concerned with the evaluation of the SIFs and the T-stress for interface cracks. The SIFs are related to the leading-order term of the expansions in Eqs. (1) and (3), while the T-stress is associated with the second term. Therefore, in the proposed XIGABEM formulation for interface cracks, we take the functions given by Eqs. (1) and (3) considering $n = 1,2$. For $n = 1$, the corresponding $\aleph_n$ is termed the complex SIF and is given by:

$$\aleph_1 = K_1 + \mathrm{i}K_2, \tag{4}$$

where K_1 and $K_2 \in \mathbb{R}$ are the modes 1 and 2 SIFs, respectively. For an interface crack of length $2a$ in an infinite body, subjected to remote stresses σ^∞ (normal to the crack surfaces) and τ^∞ (in-plane shear), the complex SIF is given by [8]:

$$K_1 + \mathrm{i}K_2 = (\sigma^\infty + \mathrm{i}\tau^\infty)\sqrt{\pi a}\,(1+2\mathrm{i}\epsilon)\,(2a)^{-\mathrm{i}\epsilon}. \tag{5}$$

Note from Eq. (5) that, unlike the homogeneous case, the SIFs cannot be unambiguously associated with the normal tension and the in-plane shear stresses. Therefore, the Arabic subscripts 1, 2 are adopted to denote these factors instead of the classical Roman numerals I, II used in the analysis of cracks in homogeneous media. Additionally, a dimensional analysis of Eq. (5) reveals that the physical units of the complex SIF are $FL^{-1.5-\mathrm{i}\epsilon}$, where F and L denote force and length, respectively. To recover the same units from the homogeneous case $\left(FL^{-1.5}\right)$, the complex SIF must be multiplied by a factor $l^{\mathrm{i}\epsilon}$, where l is an arbitrary length. Note that homogeneous relationships are recovered from the above solutions if the oscillatory parameter is taken as $\epsilon = 0$.

Using Eq. (4) and Euler's formula, the term in square brackets that appears in Eqs. (1) and (3) can be rewritten as:

$$\Re_1 \rho^{i\varepsilon} = \left[K_1 \cos(\varepsilon \log \rho) - K_2 \sin(\varepsilon \log \rho)\right] + i\left[K_1 \sin(\varepsilon \log \rho) + K_2 \cos(\varepsilon \log \rho)\right]. \tag{6}$$

For $n = 2$, after examination of the stress functions given in Appendix A, it can be observed that $Y^2_{ij}(\theta, s) = 0$ for $i, j = 1, 2$. Consequently, only the real part of $\Re_2$ is related to the T-stress term in the stress expansion. Therefore, without loss of generality, the crack parameter $\Re_2$ is adopted as:

$$\Re_2 = K_T, \tag{7}$$

where $K_T \in \mathbb{R}$ and the subscript T indicates that this factor is related to the T-stress.

Using Eq. (1), the stress functions given in Appendix A and Eq. (6), the two-term asymptotic expansion for stresses can be written as follows:

$$\sigma_{ij}(\rho, \theta, s) = \frac{1}{\sqrt{2\pi\rho}} \left\{ \Sigma^1_{ij}(\theta, s) \quad Y^1_{ij}(\theta, s) \right\} \begin{bmatrix} \cos(\varepsilon \log \rho) & -\sin(\varepsilon \log \rho) \\ \sin(\varepsilon \log \rho) & \cos(\varepsilon \log \rho) \end{bmatrix} \times \begin{Bmatrix} K_1 \\ K_2 \end{Bmatrix} + C_s T \delta_{i1} \delta_{j1}, \tag{8}$$

where $\Sigma^1_{ij}(\theta, s)$ and $Y^1_{ij}(\theta, s)$ are the stress functions for $n = 1$, δ_{ij} is the Kronecker delta and:

$$C_s = \begin{cases} \frac{(\kappa_2+1)\mu_1}{(\kappa_1+1)\mu_2}, & \text{if } s = 1 \\ 1, & \text{if } s = 2, \end{cases} \tag{9}$$

$$T = \frac{4}{\sqrt{2\pi}} \frac{(\kappa_1 + 1)\mu_2}{\left[(\kappa_1 + 1)\mu_2 + (\kappa_2 + 1)\mu_1\right]} K_T. \tag{10}$$

By examination of Eq. (8), it can be noted that the SIFs K_1 and K_2 characterise the singular and oscillatory stress field related to the distance ρ. On the other hand, the T-stress defines the homogeneous term in the expansion, with $T_1 = C_1 T$ and $T_2 = T$ representing the contribution of the normal stress parallel to the interface at the crack tip in materials 1 and 2, respectively.

Analogously, the two-term asymptotic expansion for displacements can be defined from Eq. (3) and is given by:

$$u_j(\rho, \theta, s) = \sqrt{\frac{\rho}{2\pi}} \left\{ \Delta^1_j(\theta, s) \quad \Theta^1_j(\theta, s) \right\} \begin{bmatrix} \cos(\varepsilon \log \rho) & -\sin(\varepsilon \log \rho) \\ \sin(\varepsilon \log \rho) & \cos(\varepsilon \log \rho) \end{bmatrix} \times \begin{Bmatrix} K_1 \\ K_2 \end{Bmatrix} + \frac{\rho}{\sqrt{2\pi}} \Delta^2_j(\theta, s) K_T, \tag{11}$$

where $\Delta^1_j(\theta, s)$, $\Delta^2_j(\theta, s)$ and $\Theta^1_j(\theta, s)$ are displacement functions for $n = 1, 2$ that can be computed from Appendix A.

In the expansion shown in Eq. (11), the SIFs K_1 and K_2 are related to the square-root and oscillatory behaviour of the displacement field near the tip, while the T-stress parameter K_T is associated with a linear contribution with respect to the distance ρ.

3. XIGABEM formulation for interface cracks

3.1. Boundary integral formulation for multi-region domains

For the crack analysis of domains containing different materials, we adopt the sub-region BEM technique [54,55]. Consider the inhomogeneous domain $\Omega = \Omega_1 \cup \Omega_2$ shown in Fig. 2. Each subdomain Ω_s is assumed as homogeneous, isotropic and linear elastic, and is enclosed by its respective boundary $\Gamma_s = \partial\Omega_s$, which is given by the union of the external boundary Γ^B_s, the crack surface Γ^C_s and the interface boundary Γ^I_s, i.e., $\Gamma_s = \Gamma^B_s \cup \Gamma^C_s \cup \Gamma^I_s$. Disregarding body forces, the displacement components at each point $\mathbf{x}' \in \Gamma_s$ can be computed from the following boundary integral equation (BIE):

$$c_{ij}(\mathbf{x}')u_j(\mathbf{x}') + \int_{\Gamma_s} P^*_{ij}(\mathbf{x}', \mathbf{x})u_j(\mathbf{x})d\Gamma_s = \int_{\Gamma_s} U^*_{ij}(\mathbf{x}', \mathbf{x})p_j(\mathbf{x})d\Gamma_s \qquad \mathbf{x}', \mathbf{x} \in \Gamma_s, \tag{12}$$

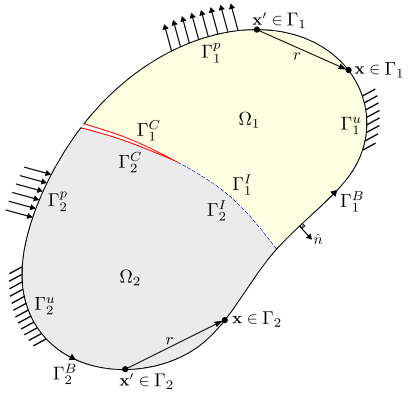

Fig. 2. Interface crack between two dissimilar materials.

in which $u_j(\mathbf{x})$ and $p_j(\mathbf{x})$ are the displacement and traction components on the boundary Γ_s, $c_{ij}(\mathbf{x}')$ is the jump term coefficient that depends on the local geometry at $\mathbf{x}'$ and is equal to $c_{ij} = \delta_{ij}/2$ for $\mathbf{x}'$ at smooth boundaries, where δ_{ij} is the Kronecker delta. $\neg\!\!\!\!\int$ denotes a singular integral to be evaluated in the Cauchy principal value sense and $U^*_{ij}(\mathbf{x}', \mathbf{x})$ and $P^*_{ij}(\mathbf{x}', \mathbf{x})$ are, respectively, the displacement and traction fundamental solutions given by:

$$U^*_{ij}(\mathbf{x}', \mathbf{x}) = \frac{1}{8\pi\mu_s(1-\nu_s)} \left[(3 - 4\nu_s)\ln\left(\frac{1}{r}\right)\delta_{ij} + r_{,i}r_{,j}\right], \tag{13}$$

$$P^*_{ij}(\mathbf{x}', \mathbf{x}) = -\frac{1}{4\pi(1-\nu_s)r} \left\{(1 - 2\nu_s)\left(r_{,j}n_i - r_{,i}n_j\right) + r_{,l}n_l\left[(1 - 2\nu_s)\delta_{ij} + 2r_{,i}r_{,j}\right]\right\}, \tag{14}$$

where $r := \|\mathbf{x}' - \mathbf{x}\|$ is the distance between the source point $\mathbf{x}' = (x'_1, x'_2)$ and the field point $\mathbf{x} = (x_1, x_2)$, n_i represents the components of the outward normal vector at $\mathbf{x}$ and $r_{,i} = \partial r/\partial x_i = (x_i - x'_i)/r$. The fundamental solutions in Eqs. (13) and (14) are valid for plane strain conditions. For plane stress states, these expressions must be used considering the modified Poisson's ratio $\bar{\nu}_s = \nu_s/(1 + \nu_s)$.

After considering a boundary discretisation, Eq. (12) can be applied independently for each subdomain to define a set of linear equations, as discussed in Section 3.6. To consider the interaction between the sub-regions, we assume that two adjacent sub-regions Ω_1 and Ω_2 are perfectly bonded at the interface boundaries Γ^I_1 and Γ^I_2. Hence, for corresponding points on the interface, each belonging to one of the materials, the following compatibility and equilibrium conditions hold:

$$\mathbf{u}^I_1 = \mathbf{u}^I_2 \qquad \text{and} \qquad \mathbf{p}^I_1 = -\mathbf{p}^I_2, \tag{15}$$

where $\mathbf{u}^I_s$ and $\mathbf{p}^I_s$ denote the displacement and traction components at a point on Γ^I_s.

3.2. NURBS basis functions

Following an isogeometric approach [56,57], we adopt the NURBS basis functions to approximate both the geometry and the mechanical fields in Eq. (12). The NURBS are a generalisation of B-splines, which are defined over a knot vector Ξ consisting of a non-decreasing sequence of real numbers in the parametric space ξ. Given the knot vector $\Xi = \{\xi_1, \xi_2, \ldots, \xi_f\}$, the B-spline functions of order p are defined by the Cox–de Boor recursion formula [58,59]:

$$N_{i,0}(\xi) = \begin{cases} 1, & \xi_i \le \xi < \xi_{i+1} \\ 0, & \text{otherwise,} \end{cases} \tag{16}$$

for $p = 0$ (constant B-spline) and:

$$N_{i,p}(\xi) = \frac{\xi - \xi_i}{\xi_{i+p} - \xi_i} N_{i,p-1}(\xi) + \frac{\xi_{i+p+1} - \xi}{\xi_{i+p+1} - \xi_{i+1}} N_{i+1,p-1}(\xi), \tag{17}$$

for $p \geq 1$. $N_{i,p}$ represents the ith B-spline function, with $i = 1, \ldots, n$, while n represents the number of basis functions defined over the parametric space $\xi \in [\xi_1, \xi_f]$. Here, we assume an open knot vector, in which the initial and final knots are repeated $p+1$ times at the start and end of Ξ. In this case, the number of entries in the knot vector is $f = n + p + 1$, and $\xi_f = \xi_{n+p+1}$.

Using the B-spline definition given in Eqs. (16) and (17) and considering a set of positive weights $\Lambda = \{w_1, w_2, \ldots, w_n\}$, in which each value w_i is associated with $N_{i,p}$, the NURBS basis functions are obtained by:

$$R_{i,p}(\xi) = \frac{N_{i,p}(\xi) w_i}{\sum_{j=1}^{n} N_{j,p}(\xi) w_j}. \tag{18}$$

When considering the isogeometric formulation, the first derivative of the NURBS basis functions is often required, and can be determined recursively by:

$$R'_{i,p}(\xi) = \frac{dR_{i,p}}{d\xi}(\xi) = w_i \frac{N'_{i,p}(\xi)\left(\sum_{j=1}^{n} N_{j,p}(\xi) w_j\right) - N_{i,p}(\xi)\left(\sum_{j=1}^{n} N'_{j,p}(\xi) w_j\right)}{\left(\sum_{j=1}^{n} N_{j,p}(\xi) w_j\right)^2}, \tag{19}$$

where $N'_{i,p}(\xi)$ is the first derivative of the B-spline functions, which are computed from:

$$N'_{i,p}(\xi) = \frac{dN_{i,p}}{d\xi}(\xi) = p\left(\frac{N_{i,p-1}(\xi)}{\xi_{i+p} - \xi_i} - \frac{N_{i+1,p-1}(\xi)}{\xi_{i+p+1} - \xi_{i+1}}\right). \tag{20}$$

Although the NURBS basis functions form a partition of unity, $\sum_{i=1}^{n} R_{i,p}(\xi) = 1$, they do not have the Kronecker delta property (i.e., $R_{i,p}(\xi_m) \neq \delta_{im}$) exhibited by the standard Lagrange polynomials used in conventional BEM. Therefore, the NURBS approximation is generally non-interpolatory at the control points. Nonetheless, the approximation is interpolatory at the start and end of the curve when considering open knot vectors.

3.3. Extended formulation

For the purpose of the isogeometric BEM analysis, a boundary element is defined in the parametric space as the span between two distinct knots, i.e., $[\xi_q, \xi_{q+1}]$, with $\xi_q \neq \xi_{q+1}$. From the recursive nature of the NURBS basis inherited from the B-splines, only the rational functions $R_{q-p,p}, R_{q-p+1,p}, \ldots, R_{q,p}$ are non-zero over the knot span. Therefore, the coordinates $\tilde{x}^e_j$, $j = 1, 2$, along an element e can be computed from:

$$\tilde{x}^e_j(\xi) = \sum_{m=1}^{p+1} \phi^{em}(\xi) x^{em}_j \qquad \xi \in [\xi_q, \xi_{q+1}] : \xi_q \neq \xi_{q+1}, \tag{21}$$

where the terms $\phi^{em}(\xi) = R_{i,p}(\xi)$ represent the mth shape function of order p from element e, with $i = m + q - p - 1$. Additionally, x^{em}_j denotes the jth coordinate of the mth local control point from element e.

In the conventional IGABEM formulation [56,57], the same approximation used in the geometry description (Eq. (21)) is applied to interpolate the displacements and tractions along the element. Therefore, similar approximations are written for the mechanical fields as follows:

$$\tilde{u}^e_j(\xi) = u^{(N)}_j(\xi) = \sum_{m=1}^{p+1} \phi^{em}(\xi) d^{em}_j, \tag{22}$$

$$\tilde{p}^e_j(\xi) = p^{(N)}_j(\xi) = \sum_{m=1}^{p+1} \phi^{em}(\xi) t^{em}_j, \tag{23}$$

where the superscript (N) emphasises that the approximations come from NURBS functions and d^{em}_j and t^{em}_j represent, respectively, the mth local displacement and traction control parameters from element e.

One issue arising from the use of the approximations in Eqs. (22) and (23) is that the NURBS basis functions fail to accurately represent the near-tip solutions for interface cracks expressed in Eqs. (1) and (3), especially the leading-order terms. To improve the numerical responses, we propose an extended formulation in which the two-term asymptotic expansions for stresses (Eq. (8)) and displacements (Eq. (11)) are used to augment the approximations over elements defining the interface and crack surfaces. Hence, the displacement approximation over an element e near a crack tip λ becomes:

$$\tilde{u}^{e\lambda}_j(\xi) = u^{(N)}_j(\xi) + T^{\lambda}_{jk} u^{(1)}_k(\mathbf{x}^{\lambda}, \mathbf{x}(\xi)) + T^{\lambda}_{jk} u^{(2)}_k(\mathbf{x}^{\lambda}, \mathbf{x}(\xi)), \tag{24}$$

where $\mathbf{x}^{\lambda}$ denotes the position of the crack tip λ, $u^{(1)}_k$ and $u^{(2)}_k$, $k = 1, 2$, are the first and second terms of the enrichment, respectively, which are expressed by:

$$\begin{Bmatrix} u^{(1)}_1 \\ u^{(1)}_2 \end{Bmatrix} = \sqrt{\frac{\rho}{2\pi}} \begin{bmatrix} \Delta^1_1(\theta, s) & \Theta^1_1(\theta, s) \\ \Delta^1_2(\theta, s) & \Theta^1_2(\theta, s) \end{bmatrix} \begin{bmatrix} \cos(\varepsilon \log \rho) & -\sin(\varepsilon \log \rho) \\ \sin(\varepsilon \log \rho) & \cos(\varepsilon \log \rho) \end{bmatrix} \times \begin{Bmatrix} \tilde{K}^{\lambda}_1 \\ \tilde{K}^{\lambda}_2 \end{Bmatrix}, \tag{25}$$

$$\begin{Bmatrix} u^{(2)}_1 \\ u^{(2)}_2 \end{Bmatrix} = \frac{\rho}{\sqrt{2\pi}} \begin{Bmatrix} \Delta^2_1(\theta, s) \\ \Delta^2_2(\theta, s) \end{Bmatrix} \tilde{K}^{\lambda}_T, \tag{26}$$

where $\rho := \|\mathbf{x} - \mathbf{x}^{\lambda}\|$, while $\tilde{K}^{\lambda}_1$, $\tilde{K}^{\lambda}_2$ and $\tilde{K}^{\lambda}_T$ represent the additional degrees of freedom included by the enrichment that are found as part of the BEM solution vector. We stress that they become accurate approximations for the SIFs and T-stress parameter only if the additional constraints to be presented in Section 3.5 are enforced at the crack tip.

The components given in Eqs. (25) and (26) are related to the local crack tip coordinate system (x'_1, x'_2), as represented in Fig. 3(a). Therefore, to express the contributions of the enrichment terms in the global coordinate system $x_1 x_2$, the components T^{λ}_{jk} from the rotation matrix are included in Eq. (24), in which:

$$\begin{bmatrix} T^{\lambda}_{11} & T^{\lambda}_{12} \\ T^{\lambda}_{21} & T^{\lambda}_{22} \end{bmatrix} = \begin{bmatrix} \cos\omega^{\lambda} & -\sin\omega^{\lambda} \\ \sin\omega^{\lambda} & \cos\omega^{\lambda} \end{bmatrix}, \tag{27}$$

where ω^{λ} is the angle between (x'_1, x'_2) and (x_1, x_2) (see Fig. 3(a)), taken positive counter-clockwise, for the crack tip λ.

To represent the near-tip singularity, the traction approximation over interface elements is also enriched with functions based on the analytical stress expansion. The enrichment terms are obtained through Cauchy's formula $p_i = \sigma_{ij} n_j$, where the stresses σ_{ij} are defined from Eq. (8) and n_j represents the outward unit normal vector at the surface. Considering a straight crack, as depicted in Fig. 3(a), the enrichment traction components – oriented according to the local crack tip coordinate system (x'_1, x'_2) – are: $p_1 = -\sigma_{12}$ and $p_2 = -\sigma_{22}$ for the upper interface surface ($s = 1$) and $p_1 = \sigma_{12}$ and $p_2 = \sigma_{22}$ for the lower interface surface ($s = 2$). Note that the second term of the stress component in Eq. (8) is related to the component σ_{11}, so there is no influence of the T-stress on the tractions along the interface. Hence, the enriched traction approximation is written as:

$$\tilde{p}^{e\lambda}_j(\xi) = p^{(N)}_j(\xi) + T^{\lambda}_{jk} p^{(1)}_k(\mathbf{x}^{\lambda}, \mathbf{x}(\xi)), \tag{28}$$

where the enrichment components $p^{(1)}_k$ are computed by:

$$\begin{Bmatrix} p^{(1)}_1 \\ p^{(1)}_2 \end{Bmatrix} = \frac{(\delta_{s2} - \delta_{s1})}{\sqrt{2\pi\rho}} \begin{bmatrix} \Sigma^1_{12}(\theta, s) & \Upsilon^1_{12}(\theta, s) \\ \Sigma^1_{22}(\theta, s) & \Upsilon^1_{22}(\theta, s) \end{bmatrix} \times \begin{bmatrix} \cos(\varepsilon \log \rho) & -\sin(\varepsilon \log \rho) \\ \sin(\varepsilon \log \rho) & \cos(\varepsilon \log \rho) \end{bmatrix} \begin{Bmatrix} \tilde{K}^{\lambda}_1 \\ \tilde{K}^{\lambda}_2 \end{Bmatrix}, \tag{29}$$

in which the expression $(\delta_{s2} - \delta_{s1})$ is included to result in -1 for $s = 1$ and $+1$ for $s = 2$. When analysing straight cracks, as illustrated in

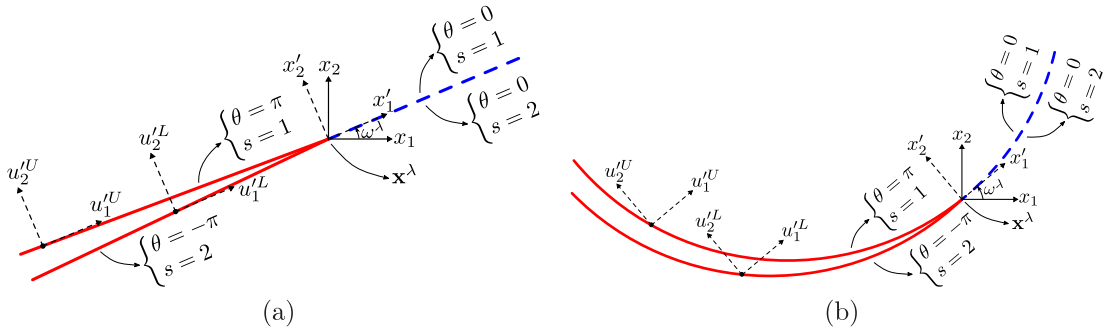

Fig. 3. Representation of (a) a straight crack and (b) a curved crack. The polar coordinates θ used in the definition of the enrichment functions over the crack and interface surfaces are equivalent in both geometries and their values are also indicated.

Fig. 3(a), the enrichment components in Eqs. (25), (26) and (29) can be simplified for the crack and interface surfaces by setting $\theta = \pm\pi$ and $\theta = 0$, respectively.

In the XIGABEM approximations shown in Eqs. (24) and (28), the enrichment terms are able to represent the near-tip solutions, while the NURBS basis functions are required to capture the difference between those near-tip solutions and the true solution over the boundary. Since this difference is a slowly varying function, the discretisation in XIGABEM can be considerably coarser than in conventional BEM, allowing a significant reduction in problem size while still obtaining highly accurate solutions.

In cases where curved cracks are considered, as illustrated in Fig. 3(b), the enrichment terms are still able to represent the near-tip solution at portions close to the crack tip since the curvature at this region is negligible. In this situation, the polar coordinate θ can be defined similarly to that of Wang et al. [60], so that its value along the crack and interface surfaces is the same as for the straight crack, as represented in Fig. 3(b). Consequently, the same enriched approximations presented above can be applied to allow the direct extraction of the tip parameters for curved cracks. While the enrichment terms capture the near-tip behaviour, the NURBS terms remain capable of representing the (still slowly varying) difference between the near-tip solutions and the true solution over the boundary. The use of the direct method is particularly beneficial in this case since the application of the interaction integral strategies, such as those based on the J-integral [40], requires the definition of auxiliary solutions considering the curvilinear nature of cracks, which is not straightforward [41,42].

In what follows, the displacement and traction approximations used over elements on the external boundary $\left(\Gamma_s^B\right)$, crack surface $\left(\Gamma_s^C\right)$ and interface $\left(\Gamma_s^I\right)$ are presented. Then, these approximations are included in Eq. (12) to define the discrete BIE for the analysis of interface crack problems.

3.3.1. Approximations over the external boundary $\left(\Gamma_s^B\right)$

The NURBS defining the external boundary Γ_s^B are not considered enriched in the proposed XIGABEM formulation. The approximations for displacements and tractions over elements at these regions are the same used in conventional IGABEM, which are presented in Eqs. (22) and (23).

3.3.2. Approximations over the crack boundary $\left(\Gamma_s^C\right)$

For elements along the crack surfaces Γ_s^C, the enriched displacement approximation can be written as:

$$\tilde{u}_j^{e\lambda}(\xi) = \sum_{m=1}^{p+1} \phi^{em}(\xi) d_j^{em} + \sum_{M=1}^{2} \tilde{K}_M^\lambda T_{jk}^\lambda \psi_{kM}^C(\mathbf{x}^\lambda, \mathbf{x}(\xi)) + \tilde{K}_T^\lambda T_{j1}^\lambda \varphi^C(\mathbf{x}^\lambda, \mathbf{x}(\xi)), \tag{30}$$

where the enrichment functions ψ_{kM}^C and φ^C are determined from Eqs. (25) and (26) considering $\theta = \pm\pi$. They are expressed as follows:

$$\begin{bmatrix} \psi_{11}^C & \psi_{12}^C \\ \psi_{21}^C & \psi_{22}^C \end{bmatrix}(\rho, s) = \sqrt{\frac{\rho}{2\pi}} \frac{\left(\delta_{s1} - \delta_{s2}\right)\left(\kappa_s + 1\right)}{\left[2\mu_s\left(1 + 4\varepsilon^2\right)\cosh\left(\pi\varepsilon\right)\right]} \begin{bmatrix} -2\varepsilon & 1 \\ 1 & 2\varepsilon \end{bmatrix} \times \begin{bmatrix} \cos\left(\varepsilon \log\rho\right) & -\sin\left(\varepsilon \log\rho\right) \\ \sin\left(\varepsilon \log\rho\right) & \cos\left(\varepsilon \log\rho\right) \end{bmatrix}, \tag{31}$$

$$\varphi^C(\rho, s) = \frac{\rho}{2\sqrt{2\pi}} \frac{\left(\delta_{s1} - \delta_{s2}\right)\left(1 + \kappa_1\right)\left(1 + \kappa_2\right)}{\left[\left(1 + \kappa_2\right)\mu_1 + \left(1 + \kappa_1\right)\mu_2\right]}, \tag{32}$$

where $s = 1$ for the upper surface and $s = 2$ for the lower surface.

In the approximation shown in Eq. (30), the first enrichment term represents the analytical oscillatory square-root behaviour for displacements near the tip, while the second describes the linear contribution related to the T-stress. Although the NURBS bases are able to capture a linearly varying function, the second term of the displacement expansion is included to extract the T-stress parameter directly from the solution vector. This requires that the additional constraint equation, introduced to accommodate the additional unknown $\tilde{K}_T^\lambda$, should be defined in a way that unambiguously specifies the T-stress and NURBS contributions so that the resulting system of equations does not become rank-deficient. In other words, the definition of general supplementary equations as, for example, by insertion of additional collocation points in the style of [47], is not sufficient to yield a determined algebraic system. Section 3.5.2 presents a constraint that can be applied to accommodate $\tilde{K}_T^\lambda$ that leads to a non-singular system, which allows the direct evaluation of the T-stress parameter.

At the crack boundary, the enrichment traction components $p_k^{(1)}$ in Eq. (29) are zero since traction-free surfaces are assumed in the near-tip solution. Consequently, the unenriched traction approximation given in Eq. (23) is sufficient for elements on crack surfaces.

3.3.3. Approximations over the interface boundary $\left(\Gamma_s^I\right)$

For elements on the interface boundary Γ_s^I, the displacement approximation is similar to the one adopted for crack elements, being expressed by:

$$\tilde{u}_j^{e\lambda}(\xi) = \sum_{m=1}^{p+1} \phi^{em}(\xi) d_j^{em} + \sum_{M=1}^{2} \tilde{K}_M^\lambda T_{jk}^\lambda \psi_{kM}^I(\mathbf{x}^\lambda, \mathbf{x}(\xi)) + \tilde{K}_T^\lambda T_{j1}^\lambda \varphi^I(\mathbf{x}^\lambda, \mathbf{x}(\xi)), \tag{33}$$

where the enrichment functions ψ_{kM}^I and φ^I are determined from Eqs. (25) and (26) considering $\theta = 0$. They are computed from:

$$\begin{bmatrix} \psi_{11}^I & \psi_{12}^I \\ \psi_{21}^I & \psi_{22}^I \end{bmatrix}(\rho) = \sqrt{\frac{\rho}{2\pi}} \frac{\kappa_1\kappa_2 - 1}{\left[\left(\kappa_1\mu_2 + \mu_1\right)\left(\kappa_2\mu_1 + \mu_2\right)\right]^{1/2}} \times \begin{bmatrix} 1 & 2\varepsilon \\ 2\varepsilon & -1 \end{bmatrix} \begin{bmatrix} \cos\left(\varepsilon \log\rho\right) & -\sin\left(\varepsilon \log\rho\right) \\ \sin\left(\varepsilon \log\rho\right) & \cos\left(\varepsilon \log\rho\right) \end{bmatrix}, \tag{34}$$

$$\varphi^I(\rho) = \frac{\rho}{2\sqrt{2\pi}} \frac{\left(1+\kappa_1\right)\left(1+\kappa_2\right)}{\left[\left(1+\kappa_2\right)\mu_1 + \left(1+\kappa_1\right)\mu_2\right]}. \tag{35}$$

Note that the displacement enrichment functions are the same regardless of whether the upper or lower material is considered, which results from the assumption of a perfectly bonded interface. Besides, the functions ψ^I_{kM} and φ^I introduce the same behaviour of the analogous enrichment functions for crack surfaces.

To represent the singular stress field at the crack tip, the enriched traction approximation over the interface elements is defined as:

$$\tilde{p}^{e\lambda}_j(\xi) = \sum_{m=1}^{p+1} \phi^{em}(\xi) t^{em}_j + \sum_{M=1}^{2} \tilde{K}^{\lambda}_M T^{\lambda}_{jk} \varpi^I_{kM}(\mathbf{x}^{\lambda}, \mathbf{x}(\xi)), \tag{36}$$

where the traction enrichment functions ϖ^I_{kM} are defined from Eq. (29) considering $\theta = 0$, being expressed by:

$$\begin{bmatrix} \varpi^I_{11} & \varpi^I_{12} \\ \varpi^I_{21} & \varpi^I_{22} \end{bmatrix}(\rho, s) = \frac{\left(\delta_{s2} - \delta_{s1}\right)}{\sqrt{2\pi\rho}} \begin{bmatrix} \sin(\varepsilon \log\rho) & \cos(\varepsilon \log\rho) \\ \cos(\varepsilon \log\rho) & -\sin(\varepsilon \log\rho) \end{bmatrix}. \tag{37}$$

Note that the traction enrichment functions ϖ^I_{kM} are singular as $\rho \to 0$. Consequently, the enriched approximation given in Eq. (36) is able to represent the singular analytical behaviour at the interface.

3.4. Discrete BIE

To introduce the approximations into the BIE, the integral over Γ_s can be subdivided into integrals over the external Γ^B_s, crack Γ^C_s and interface Γ^I_s boundaries, resulting in:

$$\begin{aligned} c_{ij}(\mathbf{x}')u_j(\mathbf{x}') + \int_{\Gamma^B_s} P^*_{ij}(\mathbf{x}', \mathbf{x})\tilde{u}_j(\mathbf{x}) d\Gamma^B_s + \int_{\Gamma^C_s} P^*_{ij}(\mathbf{x}', \mathbf{x})\tilde{u}_j(\mathbf{x}) d\Gamma^C_s \\ + \int_{\Gamma^I_s} P^*_{ij}(\mathbf{x}', \mathbf{x})\tilde{u}_j(\mathbf{x}) d\Gamma^I_s = \\ = \int_{\Gamma^B_s} U^*_{ij}(\mathbf{x}', \mathbf{x})\tilde{p}_j(\mathbf{x}) d\Gamma^B_s + \int_{\Gamma^C_s} U^*_{ij}(\mathbf{x}', \mathbf{x})\tilde{p}_j(\mathbf{x}) d\Gamma^C_s \\ + \int_{\Gamma^I_s} U^*_{ij}(\mathbf{x}', \mathbf{x})\tilde{p}_j(\mathbf{x}) d\Gamma^I_s. \end{aligned} \tag{38}$$

Then, introducing the displacement and traction approximations presented in Sections 3.3.1–3.3.3, the discrete BIE is obtained as:

$$\begin{aligned} c_{ij}(\mathbf{x}')\tilde{u}^{e'}_j(\xi') + \sum_{e=1}^{N_e} \sum_{m=1}^{p+1} P^{em}_{ij} d^{em}_j + \sum_{\lambda=1}^{N_\lambda} \sum_{M=1}^{2} \tilde{K}^{\lambda}_M \left(\sum_{e=1}^{N^{\lambda C}_e} \tilde{P}^{e\lambda C}_{iM} + \sum_{e=1}^{N^{\lambda I}_e} \tilde{P}^{e\lambda I}_{iM} \right) + \\ + \sum_{\lambda=1}^{N_\lambda} \tilde{K}^{\lambda}_T \left(\sum_{e=1}^{N^{\lambda C}_e} \tilde{P}^{e\lambda C}_{i} + \sum_{e=1}^{N^{\lambda I}_e} \tilde{P}^{e\lambda I}_{i} \right) = \sum_{e=1}^{N_e} \sum_{m=1}^{p+1} U^{em}_{ij} t^{em}_j + \sum_{\lambda=1}^{N_\lambda} \sum_{M=1}^{2} \tilde{K}^{\lambda}_M \sum_{e=1}^{N^{\lambda I}_e} \tilde{U}^{e\lambda I}_{iM}, \end{aligned} \tag{39}$$

where N_e is the number of isogeometric elements in the discretisation of Γ_s, N_λ is the number of interface crack tips and $N^{\lambda C}_e$ and $N^{\lambda I}_e$ are, respectively, the number of crack and interface elements enriched by tip λ.

The integral kernels P^{em}_{ij} and U^{em}_{ij} in Eq. (39) are exactly the same as those used in an unenriched IGABEM scheme, being given by:

$$P^{em}_{ij} = \int_{-1}^{1} P^*_{ij}(\mathbf{x}', \mathbf{x}(\hat{\xi}))\phi^{em}(\hat{\xi}) J^e(\hat{\xi}) d\hat{\xi}, \tag{40}$$

$$U^{em}_{ij} = \int_{-1}^{1} U^*_{ij}(\mathbf{x}', \mathbf{x}(\hat{\xi}))\phi^{em}(\hat{\xi}) J^e(\hat{\xi}) d\hat{\xi}, \tag{41}$$

where $J^e(\hat{\xi})$ is the Jacobian of the transformation from the parent space $\hat{\xi}$ to the Cartesian coordinate system.

The integrals in Eqs. (40) and (41) are written over the parent space $\hat{\xi} \in [-1, 1]$ for numerical integration over an isogeometric element defined in the parametric space $\xi \in \left[\xi_q, \xi_{q+1}\right]$, with parameters ξ and $\hat{\xi}$ related by:

$$\xi = \frac{\left(\xi_{q+1} - \xi_q\right)\hat{\xi} + \left(\xi_{q+1} + \xi_q\right)}{2}. \tag{42}$$

The numerical integration of Eqs. (40) and (41) can be performed following the standard IGABEM schemes. Details about the implementation of these strategies in the isogeometric BEM framework can be found in [52,56,57].

Regarding the kernels $\tilde{P}^{e\lambda C}_{iM}$ and $\tilde{P}^{e\lambda I}_{iM}$ in Eq. (39), they contain the first-order displacement enrichment functions for crack and interface elements, respectively. A general form can be written to express such terms as:

$$\tilde{P}^{e\lambda\alpha}_{iM} = \int_{-1}^{1} P^*_{ij}(\mathbf{x}', \mathbf{x}(\hat{\xi}))T^{\lambda}_{jk}\psi^{\alpha}_{kM}(\mathbf{x}^{\lambda}, \mathbf{x}(\hat{\xi}))J^e(\hat{\xi}) d\hat{\xi}, \tag{43}$$

where $\alpha = C, I$ indicates whether ψ^{α}_{kM} is evaluated at the crack (Eq. (31)) or interface boundary (Eq. (34)), respectively. Although the enrichment functions are oscillatory in nature, this behaviour is restricted to portions very close to the crack tip. Elsewhere, these functions are well behaved, which allows the use of the same integration strategies applied for the enriched integrands in XIGABEM for homogeneous domains that are detailed in Andrade et al. [52]. Nonetheless, the precision of the Gauss–Legendre quadrature is affected when integrating the oscillatory functions, particularly over the elements containing the crack tip. The influence of the accuracy of the integration over these elements on the numerical solution is investigated in Section 4.1.

The second-order displacement enrichment functions considered in the approximations of crack and interface elements introduce the integral kernels $\bar{P}^{e\lambda C}_i$ and $\bar{P}^{e\lambda I}_i$ in Eq. (39), which are related to the T-stress parameter $\tilde{K}^{\lambda}_T$. They can be expressed as:

$$\bar{P}^{e\lambda\alpha}_i = \int_{-1}^{1} P^*_{ij}(\mathbf{x}', \mathbf{x}(\hat{\xi}))T^{\lambda}_{j1}\varphi^{\alpha}(\mathbf{x}^{\lambda}, \mathbf{x}(\hat{\xi}))J^e(\hat{\xi}) d\hat{\xi}, \tag{44}$$

where $\alpha = C, I$ indicates whether φ^{α} is evaluated at the crack (Eq. (32)) or interface boundary (Eq. (35)), respectively. The enrichment term φ^{α} is a linear function, so the integral in Eq. (44) can be evaluated without further difficulty with the same strategies used for kernels containing the rational basis functions.

Finally, the extended traction approximation adopted for interface elements (Eq. (36)) introduces the integral kernel $\tilde{U}^{e\lambda I}_{iM}$ in the discrete BIE. This integral is given by:

$$\tilde{U}^{e\lambda I}_{iM} = \int_{-1}^{1} U^*_{ij}(\mathbf{x}', \mathbf{x}(\hat{\xi}))T^{\lambda}_{jk}\varpi^I_{kM}(\mathbf{x}^{\lambda}, \mathbf{x}(\hat{\xi}))J^e(\hat{\xi}) d\hat{\xi}. \tag{45}$$

Unlike the previous enrichment functions, the functions ϖ^I_{kM} in Eq. (45) are singular at the crack tip, where $\rho = 0$ (see Eq. (37)). Therefore, to evaluate the integral in Eq. (45) over elements containing the crack tip using Gauss–Legendre quadrature, the singularity $\mathcal{O}(\rho^{-0.5})$ must firstly be regularised. For this purpose, the transformation of the parent coordinate $\hat{\xi}$ presented in Appendix B is applied. It is worth mentioning that discontinuous NURBS (see [52]) are adopted to model the crack and interface surfaces so that the initial and final collocation points of the NURBS are shifted into the curve (see Fig. 4). Therefore, no collocation point is positioned at the crack tip and, consequently, the singularity present in the fundamental solution U^*_{ij} when the tip element contains the source point $\mathbf{x}'$ does not coincide with the location of the singularity in ϖ^I_{kM}.

3.5. Additional constraints

The enriched approximations used in the XIGABEM formulation contain the parameters $\tilde{K}^{\lambda}_1$, $\tilde{K}^{\lambda}_2$ and $\tilde{K}^{\lambda}_T$ that become additional degrees of freedom in the analysis. Therefore, supplementary relations are required to accommodate these enrichment parameters and yield a square linear system of equations. In what follows, we provide some additional constraints used for this purpose.

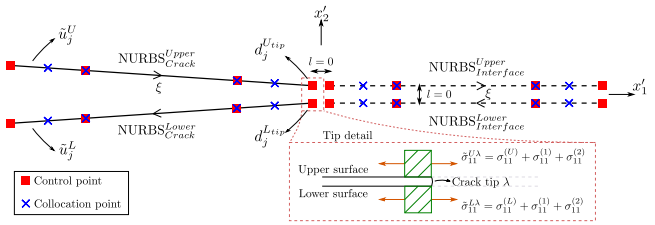

Fig. 4. Illustration of the NURBS describing the crack and interface surfaces. The displacement control parameters involved in the crack tip tying constraint are indicated. Besides, the tip detail shows infinitesimal elements with indication of the normal stress components parallel to the crack tip, which are used to define the additional equation to accommodate the T-stress parameter.

These additional equations seek to introduce some analytical conditions observed at the crack tip into the numerical solution. The use of such relations has the benefit of making the enrichment parameters into a good representation of the SIFs K_1^λ and K_2^λ and the T-stress parameters K_T^λ, since the analytical constraints are now met in the numerical method. Consequently, the crack tip factors are obtained directly from the solution of the algebraic system provided by the XIGABEM.

3.5.1. Crack tip tying constraint

To accommodate the additional parameters related to the SIFs for interface cracks, we enforce continuity of displacement at the crack tip by applying the crack tip tying constraint originally proposed by Alatawi and Trevelyan [48] for homogeneous media, and extended to the XIGABEM formulation by Andrade et al. [52]. Here, distinct NURBS are used to describe each one of the crack surfaces, as illustrated in Fig. 4. All elements on the NURBS defining both the crack and interface boundaries ending at a crack tip λ are considered enriched by the corresponding functions associated with the tip. Consequently, the displacement approximation over each crack element is given according to Eq. (30).

Consider the enriched expansion in Eq. (30) for the displacement over the crack boundary. When this is used to evaluate the displacement at the crack tip, the value of $\rho = 0$ causes the displacement enrichment functions in Eq. (31) to vanish. In addition, since open knot vectors are used, the NURBS contribution is reduced to the displacement control parameter at the tip. Therefore, the displacement continuity at the tip is reduced to the following:

$$d_j^{U_{tip}} - d_j^{L_{tip}} = 0. \tag{46}$$

where $d_j^{U_{tip}}$ and $d_j^{L_{tip}}$ are the displacement parameters related to the control points at the crack tip of the upper and lower NURBS, respectively (see Fig. 4).

Eq. (46) provides a set of two equations per crack tip that accommodate the additional enrichment parameters $\tilde{K}_1^\lambda$ and $\tilde{K}_2^\lambda$.

3.5.2. Constraint on the stress parallel to the crack tip

To accommodate the enrichment T-stress parameter, we introduce a novel constraint based on the relation between the normal stress components parallel to the interface at the crack tip, that is verified in the two-term asymptotic expansion (see detail in Fig. 4).

Similarly to displacements and tractions, the stress components over an element can also be approximated considering the NURBS and enrichment terms. Hence, the normal stress σ_{11} oriented according to the local crack tip coordinate system (x_1', x_2') can be approximated by:

$$\tilde{\sigma}_{11}^{e\lambda}(\xi) = \sigma_{11}^{(N)}(\xi) + \sigma_{11}^{(1)}(\mathbf{x}^\lambda, \mathbf{x}(\xi)) + \sigma_{11}^{(2)}(\mathbf{x}^\lambda, \mathbf{x}(\xi)), \tag{47}$$

where $\sigma_{11}^{(N)}$ is the contribution obtained from the NURBS functions and $\sigma_{11}^{(1)}$ and $\sigma_{11}^{(2)}$ are, respectively, the enrichment components obtained from the first and second terms of the near-tip stress expansion shown in Eq. (8). For elements along the crack surfaces, the enrichment terms are:

$$\sigma_{11}^{(1)}(\rho, s) = \frac{2\left(\delta_{s2} - \delta_{s1}\right)}{\sqrt{2\pi\rho}\cosh(\pi\varepsilon)}\left[\tilde{K}_1^\lambda \sin(\varepsilon \log\rho) + \tilde{K}_2^\lambda \cos(\varepsilon \log\rho)\right], \tag{48}$$

$$\sigma_{11}^{(2)}(\rho, s) = C_s T = \frac{4}{\sqrt{2\pi}} \frac{C_s\left(\kappa_1 + 1\right)\mu_2}{\left[\left(\kappa_1 + 1\right)\mu_2 + \left(\kappa_2 + 1\right)\mu_1\right]} \tilde{K}_T, \tag{49}$$

where Eq. (10) enables the last equality in Eq. (49).

Note from Eq. (48) that the singular stress component for two corresponding points (same ρ) on the upper and lower crack surfaces are equal in magnitude but opposite in sign. Therefore, the sum of the analytical stress components at these two corresponding points results only in the addition of the terms related to the T-stress, i.e., $\left(C_1 + C_2\right)T$. However, this relation between the stress components is not ensured in the XIGABEM approximation given in Eq. (47) due to the presence of the NURBS contribution $\sigma_{11}^{(N)}$. Thus, to satisfy the analytical condition at the crack tip, the sum of the NURBS terms at this point should vanish, i.e.:

$$\sigma_{11}^{(U)}(\xi_f) + \sigma_{11}^{(L)}(\xi_1) = 0, \tag{50}$$

where $\sigma_{11}^{(U)}$ and $\sigma_{11}^{(L)}$ are obtained considering the approximation over the NURBS defining the upper and lower surfaces, respectively. It is worth emphasising that Eq. (50) does not represent the definition of a new state of stress since the components are taken at different points – one in material 1 and the other in material 2 – but it is solely an expression that can be used to satisfy the analytical behaviour at the tip.

The stress components in Eq. (50) can be obtained from a generalised Hooke's law statement, and can be shown to be related to the NURBS derivatives and the displacement control parameters over the tip element e by:

$$\sigma_{11}^{(N)}(\xi_{tip}, s) = \frac{\left(\delta_{s1} - \delta_{s2}\right)E_s^*}{J^N(\xi_{tip})} \sum_{m=1}^{p+1} \frac{d\phi^{Nm}}{d\xi}(\xi_{tip})\left(d_1^{Nm}\cos\omega^\lambda + d_2^{Nm}\sin\omega^\lambda\right), \tag{51}$$

where $N = U, L$ indicates whether e is the tip element on the upper ($s = 1$) or lower ($s = 2$) surface, respectively, $J^N(\xi) = \sqrt{\left(\frac{d\tilde{x}_1^e}{d\xi}(\xi)\right)^2 + \left(\frac{d\tilde{x}_2^e}{d\xi}(\xi)\right)^2}$ is the Jacobian of the transformation, ξ_{tip} denotes the corresponding knot at the crack tip, $E_s^* = E_s$ for plane stress and $E_s^* = E_s/\left(1 - \nu_s^2\right)$ for plane strain.

Substituting Eq. (51) in Eq. (50) leads to:

$$\frac{E_1^*}{J^U(\xi_f)} \sum_{m=1}^{p+1} \frac{d\phi^{Um}}{d\xi}(\xi_f)\left(d_1^{Um}\cos\omega^\lambda + d_2^{Um}\sin\omega^\lambda\right) - \frac{E_2^*}{J^L(\xi_1)} \sum_{m=1}^{p+1} \frac{d\phi^{Lm}}{d\xi}(\xi_1)\left(d_1^{Lm}\cos\omega^\lambda + d_2^{Lm}\sin\omega^\lambda\right) = 0. \tag{52}$$

Eq. (52) provides an additional relation for each crack tip that accommodates the T-stress parameter $\tilde{K}_T^\lambda$. This expression defines a constraint on the NURBS derivatives at the tip that is sufficient to make the linear displacement enrichment related to the T-stress independent from the NURBS contribution (see Eq. (30)). Therefore, the final algebraic system becomes determined. Additionally, we note that normalising the terms in Eq. (52) by the coefficient of maximum magnitude has a beneficial effect on the conditioning of the resulting system of equations.

3.6. Assembly of the system of equations

The system of equations defined by XIGABEM is assembled considering the collocation method and the discrete form of the BIE presented in Eq. (39). In this process, the source point is chosen to lie, in turn, at each collocation point, which is defined at the Greville

abscissae [61,62]:

$$\xi'_i = \frac{\sum_{j=1}^{p} \xi_{i+j}}{p}, \tag{53}$$

where ξ'_i is the knot corresponding to the ith collocation point along the NURBS of order p. With a particular parametric coordinate ξ', the position of the corresponding collocation point $\mathbf{x}'(\xi')$ can be computed from Eq. (21).

Special attention should be given to the jump term in Eq. (39). The displacement components at the source point $\tilde{u}_j^{e'}(\xi')$ must be written considering the approximation over the element e' that contains $\mathbf{x}'$, i.e., $u_j(\mathbf{x}') = \tilde{u}_j^{e'}(\xi')$. Consequently, when assembling the system of equations, the jump term coefficients c_{ij} must be distributed over the degrees of freedom defining $\tilde{u}_j^{e'}(\xi')$, which include the enrichment parameters if e' is enriched.

After considering each collocation point in the isogeometric boundary element mesh as source point of the BIE (Eq. (39)) and carrying out the integration over the boundary $\Gamma_s = \Gamma_s^B \cup \Gamma_s^C \cup \Gamma_s^I$ that contains $\mathbf{x}'$, the following system of linear equations is determined:

$$\begin{bmatrix} \mathbf{H}_1^B & \mathbf{H}_1^C & \mathbf{H}_1^I & \mathbf{0} & \mathbf{0} & \mathbf{0} & \tilde{\mathbf{H}}_1^C + \tilde{\mathbf{H}}_1^I & \bar{\mathbf{H}}_1^C + \bar{\mathbf{H}}_1^I \\ \mathbf{0} & \mathbf{0} & \mathbf{0} & \mathbf{H}_2^B & \mathbf{H}_2^C & \mathbf{H}_2^I & \tilde{\mathbf{H}}_2^C + \tilde{\mathbf{H}}_2^I & \bar{\mathbf{H}}_2^C + \bar{\mathbf{H}}_2^I \end{bmatrix} \begin{Bmatrix} \mathbf{d}_1^B \\ \mathbf{d}_1^C \\ \mathbf{d}_1^I \\ \mathbf{d}_2^B \\ \mathbf{d}_2^C \\ \mathbf{d}_2^I \\ \tilde{\mathbf{K}} \\ \tilde{\mathbf{K}}_T \end{Bmatrix} = \tag{54}$$
$$= \begin{bmatrix} \mathbf{G}_1^B & \mathbf{G}_1^C & \mathbf{G}_1^I & \mathbf{0} & \mathbf{0} & \mathbf{0} & \tilde{\mathbf{G}}_1^I \\ \mathbf{0} & \mathbf{0} & \mathbf{0} & \mathbf{G}_2^B & \mathbf{G}_2^C & \mathbf{G}_2^I & \tilde{\mathbf{G}}_2^I \end{bmatrix} \begin{Bmatrix} \mathbf{t}_1^B \\ \mathbf{t}_1^C \\ \mathbf{t}_1^I \\ \mathbf{t}_2^B \\ \mathbf{t}_2^C \\ \mathbf{t}_2^I \\ \tilde{\mathbf{K}} \end{Bmatrix}.$$

In Eq. (54), the subscript $s = 1, 2$ denotes the subdomain, while the superscript $\alpha = B, C, I$ represents the external, crack and interface boundaries, respectively. The sub-matrices $\mathbf{H}_s^\alpha$, $\tilde{\mathbf{H}}_s^\alpha$ and $\bar{\mathbf{H}}_s^\alpha$ are defined, respectively, from the kernels P_{ij}^{em}, $\tilde{P}_{iM}^{e\lambda\alpha}$ and $\bar{P}_i^{e\lambda\alpha}$ of the BIE (39). These sub-matrices also contain the distribution of the jump terms c_{ij} over the degrees of freedom defining the displacement components at the source points. Additionally, the sub-matrices $\mathbf{G}_s^\alpha$ and $\tilde{\mathbf{G}}_s^I$ contain the coefficients determined from the integral kernels U_{ij}^{em} and $\tilde{U}_{iM}^{e\lambda I}$, respectively. Finally, the vectors $\mathbf{d}_s^\alpha$ and $\mathbf{t}_s^\alpha$ include the displacement and traction parameters at the control points, while the vectors $\tilde{\mathbf{K}}$ and $\tilde{\mathbf{K}}_T$ store the enrichment unknowns related to the SIFs and T-stress for all crack tips. Note that, since traction-free cracks are considered, $\mathbf{t}_1^C = \mathbf{t}_2^C = \mathbf{0}$.

Algorithm 1 summarises the integration process in the XIGABEM code for interface cracks. Note that, relative to the unenriched approach, only the conditional block to check whether an element is enriched must be inserted. Moreover, since a significant part of the quantities in the enriched integral kernels is already computed in the conventional BEM kernels – such as the fundamental solutions and the Jacobian – the additional calculations are reduced to the evaluation of the enrichment functions. Consequently, the extended formulation can be easily coupled to existing codes without significantly affecting computational performance.

Algorithm 1: XIGABEM for interface cracks – Integration Algorithm

```
for x' ∈ Γ_s do
    for e ∈ Γ_s do
        Compute P_ij^em   →  H_s^a;
        Compute U_ij^em   →  G_s^a;
        // obs: α = B if e ∈ Γ_s^B; α = C if e ∈ Γ_s^C; α = I
           if e ∈ Γ_s^I
        if e on a crack surface enriched by tip λ then
            Compute P̃_iM^eλC  →  H̃_s^C;
            Compute P̄_i^eλC   →  H̄_s^C;
        else if e on an interface surface enriched by tip λ then
            Compute P̃_iM^eλI  →  H̃_s^I;
            Compute P̄_i^eλI   →  H̄_s^I;
            Compute Ũ_iM^eλI  →  G̃_s^I;
        end
    end
    Compute c_ij(x')ũ_j^e'(ξ')  →  H_s^α, H̃_s^α, H̄_s^α;
end
```

In our applications, the NURBS used to describe the upper and lower interface surfaces are defined by the same knot and weight vectors and by control points located at the same position (see Fig. 4). Therefore, to satisfy the conditions of a perfectly bonded interface expressed by Eq. (15), it is sufficient to impose the following compatibility constraints for corresponding control points:

$$\mathbf{d}_1^I = \mathbf{d}_2^I \qquad \text{and} \qquad \mathbf{t}_1^I = -\mathbf{t}_2^I. \tag{55}$$

After imposing the external boundary conditions and the relations of Eq. (55) in Eq. (54), and then inserting the additional constraints given in Eqs. (46) and (52), the final the system of equations defined by XIGABEM becomes expressed as:

$$\begin{bmatrix} \mathbf{A}_1^B & \mathbf{H}_1^C & \mathbf{H}_1^I & -\mathbf{G}_1^I & \mathbf{0} & \mathbf{0} & \tilde{\mathbf{H}}_1^C + \tilde{\mathbf{H}}_1^I - \tilde{\mathbf{G}}_1^I & \bar{\mathbf{H}}_1^C + \bar{\mathbf{H}}_1^I \\ \mathbf{0} & \mathbf{0} & \mathbf{H}_2^I & \mathbf{G}_2^I & \mathbf{A}_2^B & \mathbf{H}_2^C & \tilde{\mathbf{H}}_2^C + \tilde{\mathbf{H}}_2^I - \tilde{\mathbf{G}}_2^I & \bar{\mathbf{H}}_2^C + \bar{\mathbf{H}}_2^I \\ \mathbf{0} & \hat{\mathbf{H}}_1^C & \mathbf{0} & \mathbf{0} & \mathbf{0} & \hat{\mathbf{H}}_2^C & \mathbf{0} & \mathbf{0} \end{bmatrix}$$
$$\times \begin{Bmatrix} \mathbf{y}_1^B \\ \mathbf{d}_1^C \\ \mathbf{d}_1^I \\ \mathbf{t}_1^I \\ \mathbf{y}_2^B \\ \mathbf{d}_2^C \\ \tilde{\mathbf{K}} \\ \tilde{\mathbf{K}}_T \end{Bmatrix} = \begin{Bmatrix} \mathbf{f}_1 \\ \mathbf{f}_2 \\ \mathbf{0} \end{Bmatrix}, \tag{56}$$

where $\mathbf{A}_s^B$ contains the coefficients from $\mathbf{H}_s^B$ and $\mathbf{G}_s^B$ related to the unknown control values $\mathbf{y}_s^B$ at the external boundary Γ_s^B. The vectors of constant terms $\mathbf{f}_1$ and $\mathbf{f}_2$ are given from the multiplication of the known control parameters and their corresponding influence coefficients from $\mathbf{H}_s^B$ and $\mathbf{G}_s^B$. The sub-matrices $\hat{\mathbf{H}}_s^C$ represent the additional equations introduced to accommodate the enrichment parameters, being defined by the coefficients associated with the displacement control parameters at the crack tip elements.

The solution of the linear system in Eq. (56) provides not only the unknown control variables but also the crack tip parameters introduced by the enriched formulation. Therefore, the SIFs and T-stress parameter for each crack emerge as terms in the solution vector, without requiring a post-processing technique.

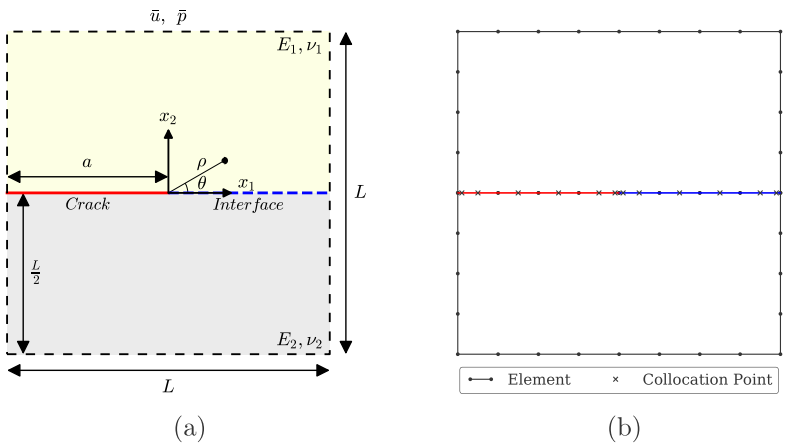

Fig. 5. (a) Bimaterial plate containing an edge interface crack. (b) Representation of the isogeometric boundary element mesh. The red and blue lines indicate the elements enriched with the crack or interface functions, respectively (Section 4.1).

4. Numerical applications

Six examples illustrate the ability of the XIGABEM formulation presented in Section 3 to directly evaluate the crack parameters for interface cracks. In the first and second applications, the accuracy is assessed with respect to available analytical solutions. In addition, the convergence of the proposed numerical formulation with mesh refinement is verified. In the last four applications, the XIGABEM solutions are compared against results of other numerical methods available in the literature. The third example also demonstrates the reduction in computation cost of the proposed direct method when compared to indirect schemes based on the J-integral.

For the XIGABEM modelling, all elements on the crack and interface surfaces are considered enriched by the tip that they define. Moreover, the order of the NURBS basis functions is selected as $p = 2$ for all analyses. Uniform isogeometric boundary element meshes are considered, in which the parametric space is subdivided in evenly spaced knots – a mesh grading scheme towards the tip or special tip elements are not required since the enrichment terms are able to capture the analytical behaviour in this region. In problems demanding increased mesh density, the h-refinement strategy is used [63]. All numerical simulations are performed on a personal notebook with AMD Ryzen™ 7 4800H @ 2.90 GHz processor and 8 GB of RAM.

In the reference solutions available in the literature, the values for the SIFs and T-stress are normalised by different terms. Where applicable, we provide the expressions used to define the normalised values.

4.1. Edge crack in a bimaterial plate

In this example, we consider a bimaterial plate with dimensions $L \times L$ containing an edge interface crack of length $a = 0.5L$, as depicted in Fig. 5(a). For the analysis, the analytical two-term expansions for both displacements and tractions are applied along the external boundary as boundary conditions. The prescribed displacement components are obtained directly from Eq. (11), while the traction values are determined from Cauchy's formula $p_i = \sigma_{ij} n_j$, with the stresses σ_{ij} given by Eq. (8). Pure mode loadings are assumed to compute the analytical boundary conditions; thus, one factor among K_1, K_2 or K_T is considered to be different from zero and equal to unity, while the other two are identically nil.

The analyses are carried out considering the enrichment of crack and interface elements with the two-term expansion. Different Young's modulus ratios $\beta = E_1/E_2$ are considered, while the Poisson's ratios for both materials are $\nu_1 = \nu_2 = 0.3$ and a plane strain condition is assumed.

The relative errors in the crack parameters for the pure mode problems are computed from:

$$e_K = \frac{\|K^{\text{ana}} - K^{\text{num}}\|}{\|K^{\text{ana}}\|} = \left\|1 - K^{\text{num}}\right\|, \tag{57}$$

where $K^{\text{ana}} = 1$ is the crack parameter considered in the pure mode and K^{num} is the corresponding numerical solution determined directly via XIGABEM.

4.1.1. Accuracy of integration

As the enrichment terms contain the expected solution for this problem and the boundary conditions are represented with a high degree of precision, the errors in XIGABEM responses are closely related to the accuracy of the numerical integration. Thus, we investigate the influence of the number of integration points used in the Gauss–Legendre quadrature on the results. Four material combinations are assumed: $\beta = 1, 2, 10$ and 100, corresponding to the oscillatory parameters $\epsilon = 0, -0.030, -0.075$ and -0.092, respectively. Pure mode problems involving only K_1 ($K_1 = 1$, $K_2 = 0$, $K_T = 0$), K_2 ($K_1 = 0$, $K_2 = 1$, $K_T = 0$) or K_T ($K_1 = 0$, $K_2 = 0$, $K_T = 1$) are addressed. The XIGABEM analyses are carried out considering a uniform boundary element mesh containing 48 isogeometric elements and 24 collocation points, as illustrated in Fig. 5(b).

Fig. 6(a) presents the relative errors, e_K, for the crack parameters – obtained directly by XIGABEM for the respective pure mode problems – with the number of integration points used for evaluation of the integrals over each element. Regarding the SIFs, the variation recovered for K_1 and K_2 are similar for every material combination since the corresponding enrichment functions and boundary conditions exhibit the same behaviour for both parameters. As for the T-stress factor, the integrals involved in the particular pure mode problem can be computed with great accuracy when using more than 20 integration points. After this threshold, the values obtained for K_T oscillate near the computational precision, with errors remaining below 10^{-13}.

The precision of the results obtained for the SIFs shown in Fig. 6(a) is directly related to the accuracy of the numerical integration over elements containing the tip. This aspect is underlined in Fig. 6(b), which shows the relative errors for the crack parameters with the number of integration points adopted for the tip elements, while a 30-point Gaussian quadrature rule is applied for elements far from the crack tip. Comparing the results from Figs. 6(a) and 6(b), when considering the homogeneous case ($\beta = 1$), the solutions are similar up to 30 integration points, indicating that the errors in the SIFs are defined by the accuracy of the numerical integrals over the tip elements. After that, the improvement of the SIFs responses in Fig. 6(b) becomes progressively smaller until a plateau is reached. In this situation, the reduction of the errors is only possible by increasing the number of

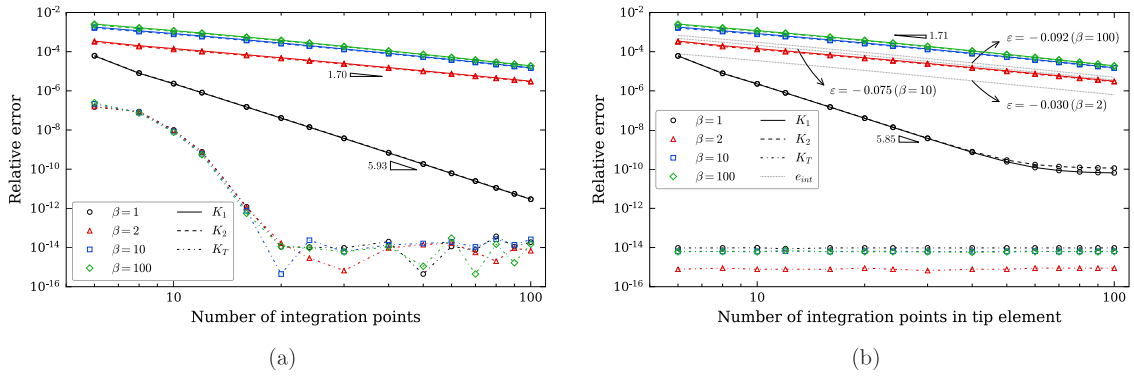

Fig. 6. Error variation of the crack parameters with the (a) number of integration points for all elements on the mesh and (b) number of integration points in the tip element while a 30-point Gaussian quadrature rule is applied for the others (Section 4.1).

Table 1
Errors for crack parameters in pure mode problems considering different boundary element meshes (Section 4.1).

β	ϵ ($\times 10^{-2}$)	n_{elem}	e_{K_1}	e_{K_2}	e_{K_T}	β	ϵ ($\times 10^{-2}$)	n_{elem}	e_{K_1}	e_{K_2}	e_{K_T}
2	−3.041	48	2.5E−5	2.3E−5	6.7E−15	100	−9.159	48	1.9E−4	1.8E−4	6.0E−15
		96	2.4E−5	2.1E−5	3.8E−14			96	1.8E−4	1.6E−4	2.6E−14
		192	2.2E−5	2.0E−5	4.9E−14			192	1.6E−4	1.5E−4	1.4E−13
		360	2.0E−5	1.8E−5	1.1E−13			360	1.5E−4	1.4E−4	2.4E−13
10	−7.581	48	1.4E−4	1.3E−4	6.2E−15	1000	−9.335	48	1.9E−4	1.8E−4	9.5E−15
		96	1.3E−4	1.2E−4	7.7E−14			96	1.8E−4	1.7E−4	6.3E−14
		192	1.2E−4	1.1E−4	1.4E−13			192	1.7E−4	1.6E−4	1.1E−13
		360	1.1E−4	1.0E−4	3.5E−13			360	1.6E−4	1.5E−4	2.5E−14

quadrature points in the whole mesh, as demonstrated by the solutions shown in Fig. 6(a).

In the inhomogeneous scenarios ($\beta > 1$), practically the same SIF results are recovered by the XIGABEM for a particular β, as shown in Figs. 6(a) and 6(b). This behaviour indicates that the errors in the numerical integration over the tip elements are dominant and control the accuracy of the solutions over the entire range of integration points. When considering material dissimilarity, the enrichment functions related to the SIFs become oscillatory. In this case, the precision of the results is strictly related to the accuracy of the quadrature used for evaluation of the integrals that contain these oscillatory terms, particularly over the tip elements. To demonstrate this, consider the integral $I = \int_0^1 \cos(\varepsilon \log z) dz$, which resembles the oscillatory enrichment terms over the elements containing the crack tip. The error in the numerical evaluation of this integral can be computed from:

$$e_{int} = \left\| 1 - \frac{I^{\text{num}}}{I^{\text{ana}}} \right\|, \tag{58}$$

where I^{num} and I^{ana} represent, respectively, the numerical and analytical solutions for I. The error e_{int} is also presented in Fig. 6(b) when considering $\epsilon = -0.030$, -0.075 and -0.092. Note that the convergence patterns obtained for the SIFs solutions and e_{int} are very similar, indicating that the errors in the XIGABEM are indeed determined by the accuracy of the numerical evaluation of the enriched kernels over the tip elements. Additionally, e_{int} increases with the magnitude of the oscillatory parameter ϵ, which is also observed in the XIGABEM responses. However, since the magnitude of ϵ is limited to an asymptotic value, the differences between solutions tend to reduce for increasing values of β.

Regarding the results for the T-stress parameter presented in Figs. 6(a) and 6(b), it is observed that the influence of the number of integration points adopted for the tip element is minimal. The enrichment functions related to K_T are linear in ρ and, therefore, the enriched integral kernels can be computed without great difficulty. Thus, when a sufficient number of quadrature points is used for evaluating all other integrals over the elements on the mesh, the errors recovered for K_T remain close to computational precision. The results show that a 30-point quadrature rule is adequate to ensure the accurate evaluation of these integrals and, therefore, we also adopt this amount of integration points in the remaining examples of this paper.

It is clear from Fig. 6(a) that high quality solutions, demonstrably of good engineering accuracy, can be obtained using a moderate number of Gauss points over all but the crack tip elements. However, we proceed with the use of a 30-point quadrature rule for the following reason. There are two main sources of error in the solution parameters: (i) the discretisation errors, which reflect how well a linear combination of NURBS and enrichment functions is able to capture the solutions, and (ii) integration errors, which affect the accuracy of matrix terms and then propagate through the solution process. We consider it most important to demonstrate in this paper the discretisation errors. A 30-point quadrature rule is chosen since it is demonstrated by the above analysis that the integration errors will be small, so that the errors presented in the remaining sections will be the important discretisation errors, i.e. not polluted by integration errors.

4.1.2. Convergence study

We now investigate the convergence of XIGABEM in the analysis of this problem with an exact solution. For this purpose, the number of isogeometric elements in the uniform boundary element mesh is varied from 48 (4 elements on the crack) to 360 (25 elements on the crack), while the parameter β assumes the following values: $2, 10, 100$ and 1000. Table 1 shows the convergence of the relative errors in the crack parameters, computed from Eq. (57), considering the respective pure mode problems. Comparing the SIF results from different material combinations, the errors tend to increase with the magnitude of the oscillatory parameter for to the same reasons identified in the previous analysis. For $\beta = 100$ and $\beta = 1000$, the solutions are practically the same as a result of the similarity between the ϵ values. Regarding K_T, the accuracy fluctuates close to computational precision.

Since the enrichment functions, on their own, are able to capture the response to the analytical problem, the contribution of the NURBS term to the final solution is minimal. Hence, the mesh refinement has little effect on the error improvement, except by slightly increasing the accuracy of the integration of oscillatory functions close to the tip, which ultimately leads to the small convergence verified for the SIFs

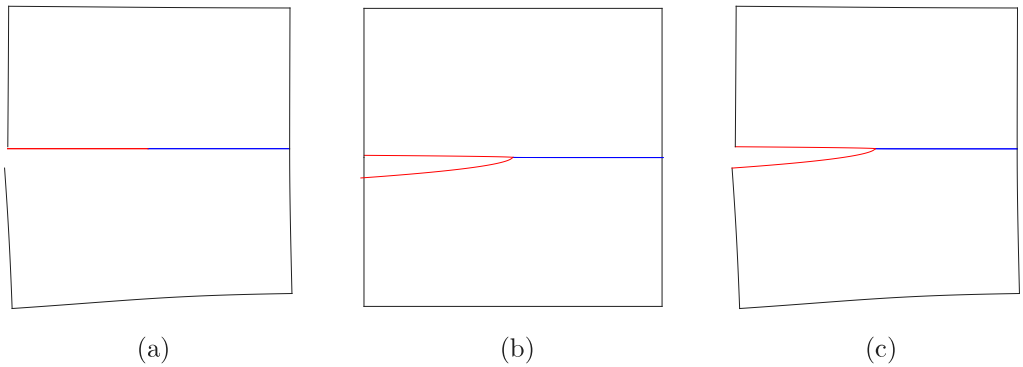

Fig. 7. (a) Deformed shape prescribed along the edges as boundary conditions and the solutions defined by the NURBS term along the crack and interface. (b) Deformed shape considering the contribution from enrichment terms for pure K_1 problem with $\beta = 10$. (c) Final deformed shape obtained by superposition of solutions (a) and (b) (Section 4.1).

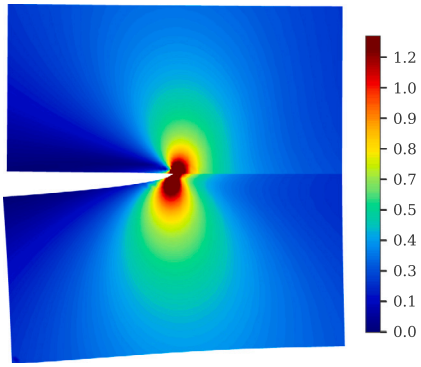

Fig. 8. Von Mises stress distribution determined by the XIGABEM for pure K_1 problem and $\beta = 10$ (Section 4.1).

in non-homogeneous scenarios. The contribution of each term of the XIGABEM approximation in the final displacement solution considering a pure K_1 problem and $\beta = 10$ is illustrated in Fig. 7. A 48-element mesh is used for the analysis. Fig. 7(a) shows the deformed shape prescribed along the edges as boundary conditions and the solutions defined by the NURBS term along the crack and interface, while Fig. 7(b) present the deformed response recovered by the enrichment terms. When these contributions are superposed, they provide the final displacement response given in Fig. 7(c). Note that the crack solution is defined by the enrichment term, whereas the NURBS term plays a minor role in the response. Finally, Fig. 8 present the von Mises stress distribution determined by XIGABEM, which clearly shows the stress concentration at the crack tip and the discontinuity in the stress field occurring at the bimaterial interface.

4.2. Curved interface crack between an inclusion and an infinite matrix

We now move on to analyse an application in which the solution is not contained in the approximation space as in the previous example. Consequently, the final response is not captured solely by the enrichment terms but also by the NURBS basis functions. Therefore, the discretisation error plays an important role in the accuracy of the XIGABEM results for this problem.

Consider an infinite matrix containing a circular inclusion of radius R and subjected to a biaxial tensile loading σ_0, as illustrated in Fig. 9(a). A curved crack with half-crack angle θ_0 is positioned along the matrix-inclusion interface. To represent the infinite matrix, we adopt $L = 100R$. For the numerical analysis, different Young's modulus ratios $\beta = E_2/E_1$ are considered, while the Poisson's ratios for both materials are taken as $\nu_1 = \nu_2 = 0.3$. A plane strain condition is considered.

Table 2
Analytical values for the crack parameters at tip B [17,64] (Section 4.2).

β:	1	2	10	100	1000
K_1^*:	0.4714	0.6288	0.8705	0.9566	0.9663
K_2^*:	−0.4714	−0.5808	−0.7147	−0.7543	−0.7586

Note: $K_1^* + \mathrm{i}K_2^* = (K_1 + \mathrm{i}K_2) / \left(\sigma_0 \sqrt{\pi} R^{0.5-\mathrm{i}\epsilon}\right)$

Initially, we study the convergence of the crack parameters at tip B considering $\theta_0 = 90°$ and taking $\beta = 1, 2, 10, 100$ and 1000, values that correspond to $\epsilon = 0$, 0.030, 0.075, 0.092 and 0.093, respectively. The number of elements in the discretisation of the interface and crack surfaces is varied from 96 to 360, while the outer boundary mesh is fixed at 40 elements. Fig. 9(b) shows the detail of the discretisation around the inclusion for the coarsest mesh. The SIFs are normalised by $K_1^* + \mathrm{i}K_2^* = (K_1 + \mathrm{i}K_2) / \left(\sigma_0 \sqrt{\pi} R^{0.5-\mathrm{i}\epsilon}\right)$, and Table 2 provides the analytical solutions [17,64] used to verify the accuracy of the XIGABEM results. The convergence curves of the SIF values are shown in Fig. 10. The errors in K_1^* decrease for increasing values of β (and ϵ), whereas the opposite behaviour is observed for K_2^*. Nevertheless, similarly to the previous example, the variations in the SIF errors with β reduce as the oscillatory parameter ϵ tends to its asymptotic value. Fig. 10 also shows the error convergence in the T-stress value at the inclusion (material 2) considering $\beta = 1$, in which the normalised reference solution is $T_2/\sigma_0 = 0.6667$ [65]. To the best of the authors' knowledge, no analytical solution is available for the T-stress in the non-homogeneous case. Accurate solutions are obtained by the direct XIGABEM formulation for both SIFs and T-stress, with errors below 0.8% even for a coarse mesh, and the convergence pattern of the solutions demonstrates the stability of the proposed method.

Figs. 11(a) and 11(b) show, respectively, the displacement contributions of the NURBS and enrichment terms, while the superposition of these two responses provides the final solution given in Fig. 11(c). Discontinuous NURBS are used to define each quarter of the inclusion, with those on the upper half enriched by tip A and those on the lower half enriched by tip B. Note that very close to the crack tips, the solution is mainly captured by the enrichment term. However, for points away from the tip, the NURBS have a significant contribution to the response, being responsible for correcting the enriched solution to account for the curvature effect. With mesh refinement, the responses from the NURBS term become more accurate, leading to the convergence of the crack parameters results shown in Fig. 10.

We now investigate the influence of the half-crack angle on the SIFs and T-stress values. For this purpose, the parameter θ_0 is varied from 5° to 175° in steps of 5°. The analyses are carried out considering a total of 232 isogeometric elements in the boundary discretisation. Fig. 12(a) presents the discrete results for the SIFs determined directly

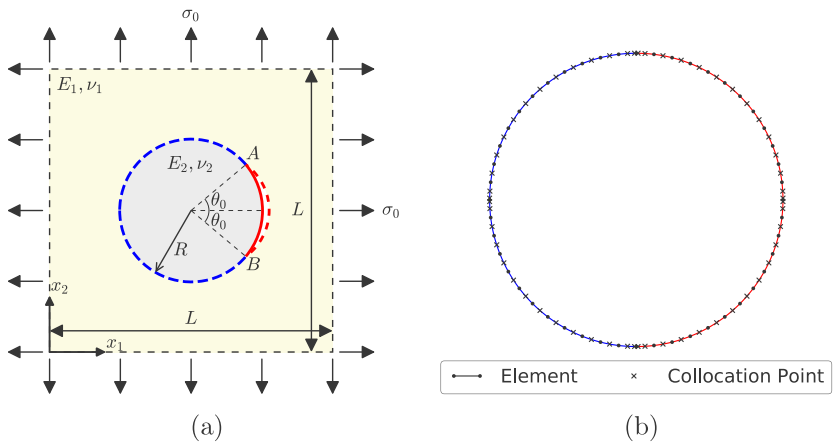

Fig. 9. (a) Infinite matrix containing an inclusion subjected to biaxial traction. (b) Detail of the isogeometric boundary element mesh around the inclusion. The red and blue lines indicate the elements enriched with the crack or interface functions, respectively (Section 4.2).

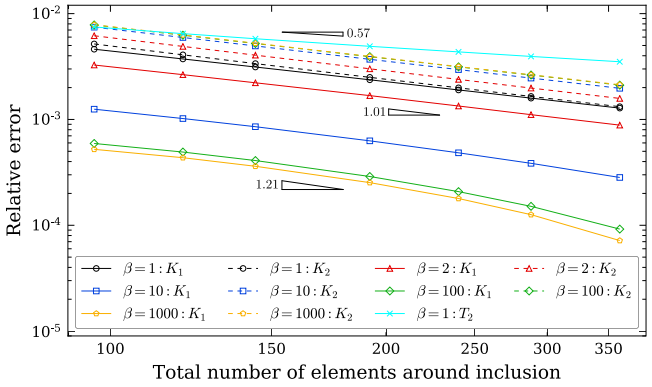

Fig. 10. Error convergence of the crack parameters solutions defined directly by XIGABEM (Section 4.2).

by XIGABEM. The analytical solutions for K_1^* and K_2^* are also given and are represented in solid and dashed lines, respectively. Excellent agreement is observed between the numerical and reference results in the whole range of θ_0. The responses for the T-stress are also determined and are shown in Fig. 12(b). Note that both the SIFs and T-stresses tend to be limited as ϵ approaches its asymptotic value. Fig. 12(b) also presents the analytical solutions of the T-stress for the homogeneous case, which, again, have excellent correspondence with the XIGABEM results.

4.3. Edge interface crack in a bimaterial strip

Consider a bimaterial strip composed of two layers of thickness h and containing an edge crack of length a. The strip is constrained at the right end, while a load of magnitude σ_0 is applied at the left end of the layers, as indicated in Fig. 13. The dimensions are taken as $L = 10h$, $a = 0.5L$ and a plane strain condition is assumed in the analyses. Initially, different material combinations are considered for the strip and the results are compared against reference solutions. Then, the convergence and computational cost of the proposed direct method are evaluated against an indirect method in which interaction integrals are used for crack parameter extraction.

4.3.1. Variation of material properties

In this analysis, four different combinations of material parameters are considered, and the values adopted for each case are shown in Table 3. Table 3 also presents the SIFs and T-stress values computed directly by XIGABEM considering a uniform boundary mesh containing 264 isogeometric elements (30 elements on each crack surface). The normalised SIF values are determined by $K_1^* + \mathrm{i}K_2^* = \left(K_1 + \mathrm{i}K_2\right) / \left(\sigma_0 \sqrt{\pi} h^{0.5-\mathrm{i}\epsilon}\right)$. Other solutions available in the literature are also shown. The results given by Suo and Hutchinson [16] for SIFs and Kim and Vlassak [18] for T-stress are determined from semi-analytical expressions considering a bimaterial strip with infinite length. On the other hand, the numerical solutions for the T-stress obtained by Yu et al. [29] (XFEM) and Muthu et al. [66] (Element-free Galerkin) are also obtained considering a finite strip of length $L = 10h$. Excellent agreement is found between the solution determined by the proposed direct method and the reference results. Particularly, when compared to the semi-analytical solutions provided by Suo and Hutchinson [16] and Kim and Vlassak [18], the errors obtained by the XIGABEM are smaller than 1%, demonstrating the accuracy of the proposed direct method in evaluating the crack parameters.

4.3.2. Comparison between the direct method and the indirect method

To compare the performance of the direct and indirect methods for evaluating the crack tip parameters, we assume the material properties from Case 1 given in Table 3. The direct solutions for the SIFs and T-stress are obtained directly via the proposed XIGABEM formulation, while the indirect results are computed through a post-processing strategy using the interaction integrals based on the J-integral [24,25]. The interaction integrals are computed along a circular path centred at the crack tip and discretised into 32 isogeometric elements.

Firstly, a convergence study is carried out by varying the number of elements in the boundary mesh and the results are presented in Figs. 14(a) and 14(b). Note that both the direct and indirect solutions converge towards the range of values found in the literature (see Table 3), indicating that the XIGABEM can provide solutions as accurate as the ones given by methods based on interaction integrals. Nevertheless, the proposed method still has the advantage of eliminating the post-processing step for the computation of the crack tip parameters (see Fig. 14).

To quantify the amount of computational effort saved by the direct method when compared to the indirect approach, the run times obtained during the convergence analyses are presented in Fig. 15. The relative difference curve is also shown. It can be noted that, by dismissing the use of internal points for computing the crack tip parameters, the proposed XIGABEM is able to reduce by 25 to 35% the execution times obtained by the indirect method. This reduction is in accordance with previous results determined by the authors in the application of the XIGABEM for homogeneous media [52]. Since the number of enriched elements increases at the same rate as the total number of elements, the growth rate in the computational time in the direct approach is close to the standard BEM, which is equal

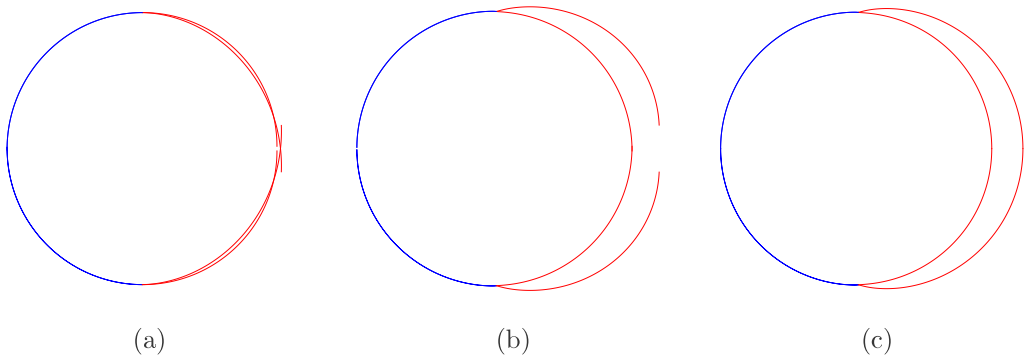

Fig. 11. Deformed shape considering the contribution from (a) NURBS basis functions and (b) enrichment terms. (c) Final deformed shape obtained by superposition of solutions (a) and (b) (Section 4.2).

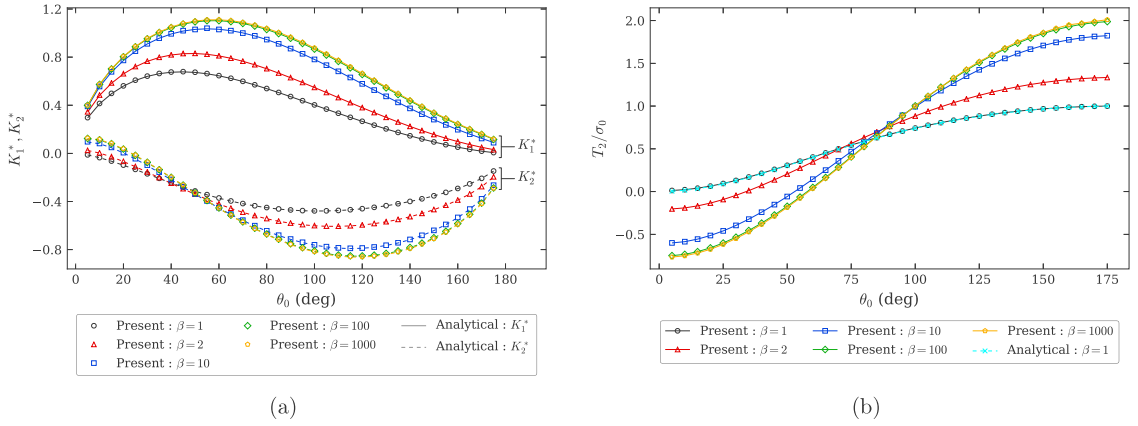

Fig. 12. (a) Normalised SIFs with the half-crack angle. Note: the continuous and dashed lines represent the analytical distributions for K_1^* and K_2^*, respectively, while the dots represent the solutions determined numerically in the present study. (b) Variation of the T-stress with the half-crack angle (Section 4.2).

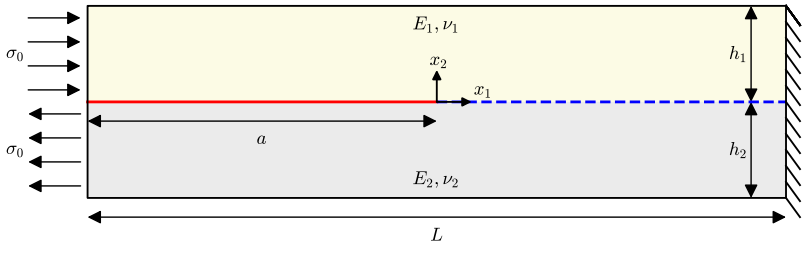

Fig. 13. Bimaterial strip with an edge interface crack (Section 4.3).

Table 3
Normalised SIFs and T-stress in material 1 for bimaterial strip with edge crack (Section 4.3).

Case	$\frac{E_1}{E_2}$	ν_1	ν_2	K_1^*		K_2^*		T_1/σ_0			
				Ref. [16]	Present	Ref. [16]	Present	Ref. [18]	Ref. [29]	Ref. [66]	Present
1	7/3	1/3	1/3	−0.0528	−0.0526	0.2976	0.2963	0.0709	0.0702	0.0709	0.0706
2	20/9	1/4	1/8	−0.0282	−0.0285	0.3056	0.3038	0.0784	0.0773	0.0778	0.0792
3	4	2/5	2/5	−0.1033	−0.1032	0.3153	0.3142	0.1310	0.1317	0.1301	0.1301
4	4	1/4	1/4	−0.0783	−0.0781	0.3277	0.3259	0.1424	0.1410	0.1419	0.1432

Note: $K_1^* + \mathrm{i}K_2^* = \left(K_1 + \mathrm{i}K_2\right) / \left(\sigma_0 \sqrt{\pi} h^{0.5-\mathrm{i}\varepsilon}\right)$

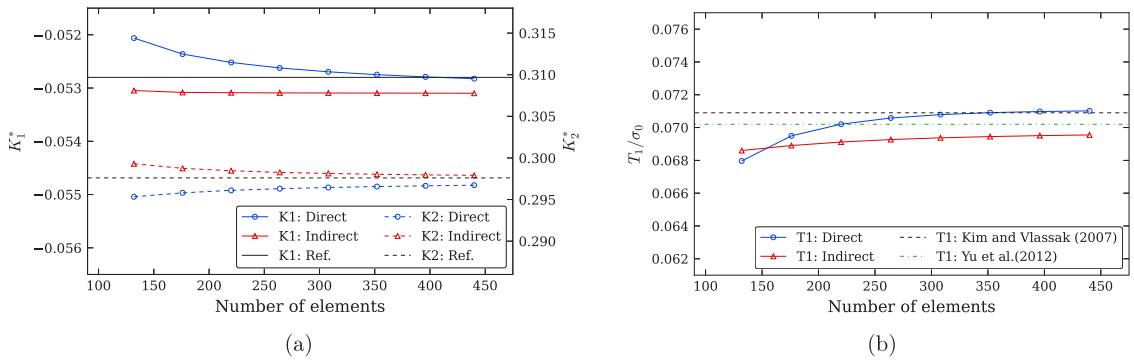

Fig. 14. Convergence of normalised (a) SIFs and (b) T-stress in material 1 with refinement of the boundary element mesh. The *Direct* results are obtained directly from the solution vector provided by the XIGABEM, while the *Indirect* responses are determined in a post-processing strategy based on interaction integrals (Section 4.3).

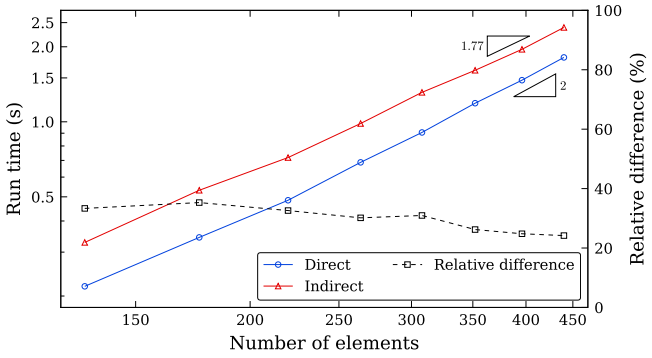

Fig. 15. Variation of execution times, in seconds, with boundary mesh refinement and relative differences, in percentage, between run times from the direct and indirect methods (Section 4.3).

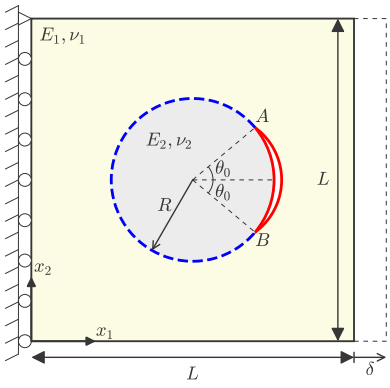

Fig. 16. Circular crack around an inclusion in a square plate (Section 4.4).

to 2. The lower growth rate observed in the indirect approach is due to the fixed number of elements used in the discretisation of the path to calculate the interaction integrals, regardless of mesh refinement. Improved computational performance can be achieved by the direct method by enriching fewer crack and interface elements. Since the analytical behaviour is predominant in regions close to the tip, the elements enriched by the crack functions can be restricted to this region, decreasing the computational effort for the calculation of enriched integral kernels.

4.4. Curved interface crack between the inclusion and matrix in a finite plate

In this example, we consider a square plate of unit length ($L = 1$) composed of a matrix of material 1 and an inclusion of material 2. In the interface between the inclusion and the matrix, there is a circular crack with a half-crack angle θ_0, as illustrated in Fig. 16. The volume fraction of the inclusion is 20%, so its radius is given by $R = \sqrt{0.2/\pi}$. The displacements in the x_1 direction are constrained along the left edge, while a constant displacement $u_1 = \delta = 0.01$ is prescribed at the right edge. Two cases are analysed: in the first one (4.4.1), the SIFs determined by the XIGABEM are compared with reference results, while in the second (4.4.2), the accuracy of the T-stress solutions is assessed. For all analyses, a plane strain condition is considered. Additionally, 184 elements are used in the boundary element discretisation (10 at each side of the plate and 72 along the perimeter of the inclusion).

4.4.1. Stress intensity factors

In this scenario, the following material properties are considered for the numerical analysis: $E_1 = 72.4 \times 10^3$, $\nu_1 = 0.22$, $E_2 = 3.45 \times 10^3$ and $\nu_2 = 0.35$. Additionally, the half-crack length θ_0 varies from 10° to 60°. Fig. 17 shows the results obtained for the SIFs normalised by $\sigma_{ave}\sqrt{\pi R\theta_0}$, where σ_{ave} is the average normal stress on the right edge of the plate. The solutions determined by Liu and Xu [34] using BEM and by Wu et al. [67] using XFEM are also provided for comparison. Good correspondence is observed between the XIGABEM solutions and the reference results, especially with those given by Wu et al. [67]. Similarly to the XFEM solutions, the curves determined by XIGABEM vary more smoothly than those obtained by conventional BEM, which indicates that the enriched formulation contributes to the stability of the results.

4.4.2. T-stress

For the T-stress analysis of the problem illustrated in Fig. 16, we consider different ratios between the Young's modulus of the inclusion and matrix, defined as $\beta = E_2/E_1$. The ratio β is taken as 0.25 (soft inclusion), 1.0 (homogeneous) and 4.0 (hard inclusion), while the Poisson's ratios for the materials are $\nu_1 = \nu_2 = 0.3$. Additionally, the half-crack angle range θ_0 is considered in the range 10° to 90°.

The results for the normalised T-stress in material 1 obtained directly by XIGABEM are presented in Fig. 18. Due to the symmetry, the T-stress values in the matrix for both tips are the same. For small cracks, T_1 tends to be a compressive stress, but as the crack length increases, T_1 becomes a tensile stress. Moreover, apart from the values of θ_0 around 40° where T_1 switches from a compressive to a tensile stress, the magnitude of T_1 is greater the stiffer the matrix is than the inclusion. Yu et al. [29] also analysed this problem using the XFEM, and their solutions are shown in Fig. 18. Good agreement is

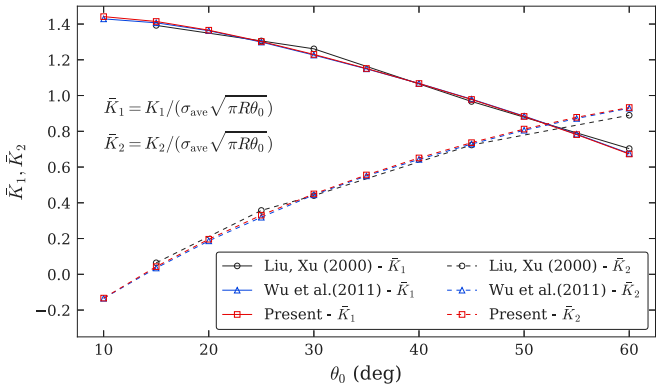

Fig. 17. Variation of the normalised SIFs at tip A with the half-crack angle θ_0 (Section 4.4).

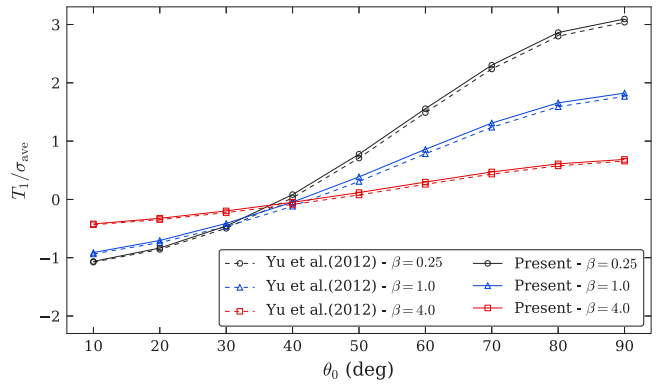

Fig. 18. Variation of the normalised T-stress in material 1 with the half-crack angle θ_0 (Section 4.4).

attained between the XIGABEM and XFEM results for different material combinations. The small differences between the solutions are of the same order of magnitude as in the previous example, in which the solutions given by Yu et al. [29] were also taken for comparison.

4.5. Bimaterial plate with a centre interface crack

Consider the bimaterial plate containing a centre crack lying along an inclined interface, as illustrated in Fig. 19. The plate has dimensions $2w \times 2h$ and is tensioned by a uniform load σ_0. The crack length is such that $a/w = 0.5$. In this example, we undertake two different analyses: firstly, we assume a horizontal interface ($\alpha = 0°$) and investigate the variation of the SIFs and T-stress for different material properties. Secondly, we study the influence of the interface slope α and the ratio E_1/E_2 on the values of the crack parameters. The SIF solutions are given in normalised form given by $K_1^* + \mathrm{i}K_2^* = \left(K_1 + \mathrm{i}K_2\right) / \left[(2a)^{-\mathrm{i}\epsilon}\sigma_0\sqrt{\pi a}\right]$, while the normalised T-stress is obtained by $T^* = T\sqrt{\pi a}/K_0$, with $K_0 = \sqrt{K_1^2 + K_2^2}$. All analyses are carried out considering 200 isogeometric elements in the boundary discretisation, with 20 elements on each crack surface.

4.5.1. Horizontal interface ($\alpha = 0°$)

For the configuration of a horizontal interface ($\alpha = 0°$), the SIFs and T-stress are computed for the ratio between Young's moduli $E_1/E_2 = 1, 2, 5$ and 10. The Poisson's ratios for both materials are $\nu_1 = \nu_2 = 0.3$ and a plane strain condition is assumed.

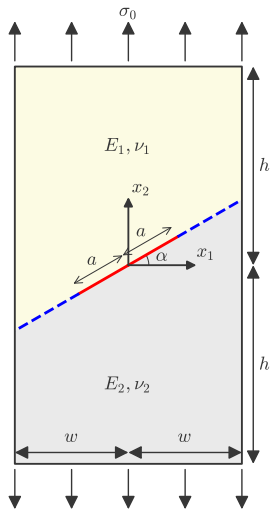

Fig. 19. Tensioned bimaterial plate containing a centre interface crack (Section 4.5).

Table 4 presents the normalised values obtained for the SIFs and T-stress in material 2. The XIGABEM solutions are compared with published results obtained with SBFEM [45] and with xSBFEM [46], which are also presented in Table 4. Excellent agreement is observed between the results for all considered combinations of material properties. This demonstrates the accuracy of the proposed direct approach for computing the interface crack parameters, especially as it performs well in comparison with the SBFEM formulation, which is acknowledged to benefit in the analysis of fracture problems from naturally capturing the asymptotic fields near the tip.

4.5.2. Inclined interface ($\alpha = 0°$-$60°$)

The inclination angle α of the interface in the bimaterial plate shown in Fig. 19 is now varied from 0° to 60°, while the ratio between Young's moduli is fixed at $\beta = E_1/E_2 = 10$ and $\nu_1 = \nu_2 = 0.3$. The analyses are carried out considering a plane stress condition.

Figs. 20(a) and 20(b) show the results for the normalised SIFs and T-stress in material 2 determined for the right and left tips, respectively. Unlike the homogeneous case (see Portela et al. [68]) the crack parameters computed for the two tips are distinct because of the material dissimilarity. The figures also present the variation of the SIFs obtained by Wang et al. [44] using XFEM and the BEM solutions provided by Miyazaki et al. [24] and Gu and Zhang [35] considering $\alpha = 15°, 30°, 45°$ and 60°. To compute the SIFs, Wang et al. [44] used Irwin's crack closure integral, Gu and Zhang [35] adopted the displacement extrapolation method combined with a crack-tip element strategy and Miyazaki et al. [24] applied a conservation integral. In these references, the K_2^* responses appear with the opposite sign than shown here due to the convention adopted in the definition of this factor. Again, the XIGABEM results are in good agreement with the solutions found in the literature, demonstrating the accuracy of the proposed direct method. Particularly, when compared to the XFEM [44], the SIF values obtained here better approximate the BEM solutions given by Miyazaki et al. [24] and Gu and Zhang [35]. Regarding the T-stress, it can be noted that for both tips this stress term changes from compression to tension as the inclination of the interface increases.

Considering the inclination angle of the interface as $\alpha = 15°, 30°, 45°$ and 60°, we also address the scenarios in which $E_1/E_2 = 100$ and $E_1/E_2 = 1000$. Table 5 shows the results obtained by the XIGABEM model and those provided by Gu and Zhang [35], including the case $E_1/E_2 = 10$ plotted in Figs. 20(a) and 20(b). Again, the XIGABEM solutions are in excellent agreement with those provided by the reference, the average difference between the solutions being around 0.4%. We

Table 4
Normalised SIFs and T-stress in material 2 for bimaterial plate with a horizontal centre crack (Section 4.5).

$\frac{E_1}{E_2}$	K_1^*			K_2^*			T_2^*		
	Ref. [45]	Ref. [46]	Present	Ref. [45]	Ref. [46]	Present	Ref. [45]	Ref. [46]	Present
1	1.1890	1.1893	1.1901	0.0000	0.0000	0.0000	−1.0600	−1.0552	−1.0531
2	1.1790	1.1798	1.1807	−0.0550	−0.0566	−0.0543	−0.7180	−0.7144	−0.7131
5	1.1480	1.1483	1.1494	−0.1040	−0.1053	−0.1041	−0.3790	−0.3770	−0.3760
10	1.1230	1.1237	1.1249	−0.1230	−0.1240	−0.1234	−0.2160	−0.2147	−0.2139

Note: $K_1^* + \mathrm{i}K_2^* = (K_1 + \mathrm{i}K_2) \,/\, \left[(2a)^{-\mathrm{i}\varepsilon}\sigma_0\sqrt{\pi a}\right]$ and $T^* = T\sqrt{\pi a}/K_0$, with $K_0 = \sqrt{K_1^2 + K_2^2}$

Table 5
Normalised SIFs and T-stress in material 1 for bimaterial plate with a horizontal centre crack (Section 4.5).

$\frac{E_1}{E_2}$	α (°)	Right tip					Left tip				
		Ref. [35]		Present			Ref. [35]		Present		
		K_1^*	K_2^*	K_1^*	K_2^*	T_2^*	K_1^*	K_2^*	K_1^*	K_2^*	T_2^*
10	15	1.1269	0.0852	1.1280	0.0860	−0.1775	1.0096	0.4440	1.0123	0.4458	−0.1991
	30	0.9924	0.2949	0.9928	0.2955	−0.1205	0.7843	0.6246	0.7871	0.6260	−0.1300
	45	0.7656	0.4061	0.7671	0.4068	−0.0257	0.5217	0.6730	0.5222	0.6739	0.0136
	60	0.4919	0.4059	0.4928	0.4060	0.1647	0.2772	0.5810	0.2779	0.5808	0.2636
100	15	1.1155	0.0590	1.1189	0.0611	−0.0198	0.9680	0.4768	0.9672	0.4799	−0.0233
	30	1.0048	0.2619	1.0079	0.2635	−0.0131	0.7543	0.6540	0.7542	0.6563	−0.0146
	45	0.8029	0.3556	0.8051	0.3563	−0.0020	0.5389	0.6957	0.5399	0.6967	0.0058
	60	0.5284	0.3290	0.5312	0.3304	0.0255	0.3498	0.5879	0.3520	0.5898	0.0483
1000	15	1.1164	0.0574	1.1176	0.0590	−0.0020	0.9597	0.4811	0.9610	0.4836	−0.0024
	30	1.0075	0.2596	1.0095	0.2601	−0.0013	0.7493	0.6583	0.7502	0.6596	−0.0015
	45	0.8065	0.3471	0.8090	0.3480	−0.0002	0.5454	0.6965	0.5466	0.6976	0.0007
	60	0.5221	0.3055	0.5271	0.3086	0.0029	0.3691	0.5749	0.3727	0.5792	0.0056

Note: $K_1^* + \mathrm{i}K_2^* = (K_1 + \mathrm{i}K_2) \,/\, \left[(2a)^{-\mathrm{i}\varepsilon}\sigma_0\sqrt{\pi a}\right]$ and $T^* = T\sqrt{\pi a}/K_0$, with $K_0 = \sqrt{K_1^2 + K_2^2}$

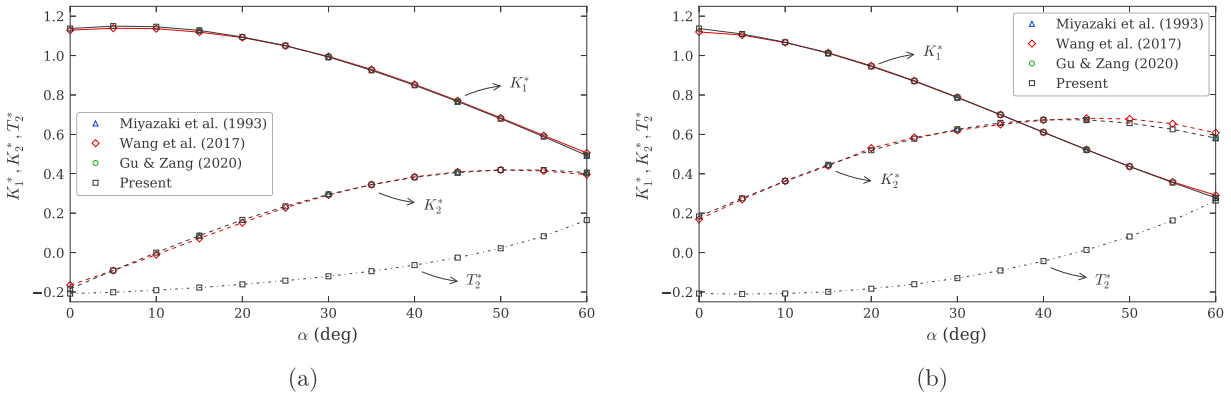

Fig. 20. Variation of the normalised SIFs and T-stress in material 2 with the interface orientation α for the (a) right tip and (b) left tip. The XIGABEM results are compared against the numerical solutions provided by Miyazaki et al. [24], Wang et al. [44] and Gu and Zhang [35] (Section 4.5).

note that the results shown here are obtained with a coarser mesh than in Gu and Zhang [35]. While 272 quadratic Lagrange elements were used in the reference, including 40 discontinuous elements along each crack surface, 200 quadratic isogeometric elements are applied here, which represents a substantial reduction in the number of degrees of freedom. The results for the T-stress in material 2 are also shown in Table 5 for completeness. It can be observed that the magnitude of T_2^* reduces as material 1 becomes relatively stiffer.

4.6. Asymmetric interface cracks between a circular inclusion and the matrix

For the last example, consider the problem of two asymmetrical circular cracks along the matrix-inclusion interface under uniform traction σ_0 at infinity, as depicted in Fig. 21. The half-crack angle of the right and left cracks are γ_1 and γ_2, respectively. We assume a fixed $\gamma_2 = 30°$, while γ_1 varies in the range 5°-55°. To simulate the infinite matrix condition and reduce the finite length effect in the numerical solutions, we adopt $L = 40R$. For each crack geometry, two material combinations are considered: the first contains a hard inclusion ($E_2 = 10E_1$, $\nu_1 = 0.3$ and $\nu_2 = 0.2$), while the second has a soft inclusion ($E_1 = 10E_2$, $\nu_1 = 0.3$ and $\nu_2 = 0.2$). Le et al. [69] derived semi-analytical expressions of the SIFs for this problem, which are used for comparison against our direct XIGABEM solutions. The isogeometric boundary element mesh considered in the numerical analysis is composed of 184 elements: 10 at each side of the plate and 72 along the perimeter of the inclusion.

The results obtained by XIGABEM for the normalised SIFs of tips A and C with the variation of γ_1 are shown in Figs. 22(a) and 22(b) for the cases of a hard inclusion and a soft inclusion, respectively. For comparisons with the solutions given by Le et al. [69], the normalised SIFs are computed by $K_1^* + \mathrm{i}K_2^* = (K_1 + \mathrm{i}K_2) \,/\, \left(\sigma_0\sqrt{2}R^{0.5+\mathrm{i}\varepsilon}\right)$. For tip A, in both material combinations, the value of K_1^* increases for small values of γ_1, reaches a maximum and then decreases with the growth of the right crack. On the other hand, K_2^* grows monotonically with increments in γ_1. For tip C, located in the crack that remains of fixed length, the values of the SIFs are reduced as the right crack increases

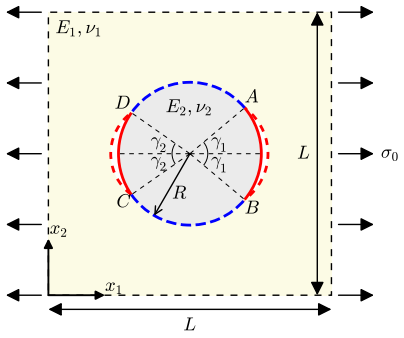

Fig. 21. Asymmetrical cracks around a circular inclusion (Section 4.6).

and becomes dominant. Additionally, when $\gamma_1 = 30°$, both cracks have the same size and the SIFs recovered for tips A and C are equal. Apart from the sign of K_2^*, the solutions for tips B and D (not shown) are equivalent to tips A and C, respectively.

Figs. 22(a) and 22(b) also present the semi-analytical and numerical SIF solutions provided by Le et al. [69]. In general, when compared to the FEM solutions given by the reference, the present results better approximate the semi-analytical responses, which demonstrates the efficiency of the proposed direct XIGABEM to determine the SIFs for interface cracks (see Fig. 22).

Finally, for the sake of completeness, we also provide the T-stress results in the inclusion determined by the direct XIGABEM for the cases of a hard inclusion (Fig. 23(a)) and a soft inclusion (Fig. 23(b)). Like the SIFs, the T-stress magnitude also reduces for the soft inclusion case since the stress level near the interface cracks decreases when the matrix is stiffer. Moreover, for both the hard and soft inclusion cases, the T-stress in material 2 for the right crack changes from compressive to tensile as γ_1 increases. For the fixed-length crack, the T-stress varies less than for the right crack and remains as a compressive stress throughout the range considered for γ_1. Again, due to the symmetry at $\gamma_1 = \gamma_2 = 30°$, the results of the T-stress parameter for both cracks are the same at this point.

5. Concluding remarks

This paper presents a novel XIGABEM formulation for the direct evaluation of the SIFs and T-stress of interface cracks, without the requirement for J-integral or M-integral type post-processing. This has been enabled by introducing singular traction enrichment functions, and by developing a novel constraint equation relating to the normal stress component parallel to the interface at the crack tip. The proposed extended formulation can be easily included into existing isogeometric BEM codes without significantly increasing the computational cost. On the contrary, the computational cost will be reduced markedly because of the ability of the enriched scheme to obtain accurate solutions from coarse meshes.

Although the direct XIGABEM formulation is based on the analytical solution for a crack lying in a straight interface, it is also successfully employed for the analysis of curved cracks since the asymptotic behaviour can be captured by the same enrichment functions. Besides, the use of NURBS functions in the XIGABEM formulation allows the exact description of certain curved geometries, including cracks and interfaces, which minimises the errors associated with geometric approximation.

The numerical applications presented in Section 4 demonstrate the stability and accuracy of the direct XIGABEM for the analysis of interface cracks. A detailed study was made of the influence of the oscillatory enrichment functions on the precision of numerical integration for different quadrature orders, and the convergence of the method was investigated for different material combinations. Excellent agreement was attained between the XIGABEM results and the reference solutions available in the literature. Furthermore, it has been shown that the execution time of the direct method is significantly lower than that of the interaction integral method.

It is worth mentioning that the two-term enrichment strategy can also be applied to homogeneous materials so that the SIFs and T-stress can also be obtained directly from the solution vector. The further consideration of anisotropic materials and the extension of the method to 3D problems can also be investigated, and such applications are work in progress. The prospect of accurate predictions for the crack parameters in 3D without the expense of multiple evaluations of interaction integrals is highly appealing.

Declaration of competing interest

The authors declare that they have no known competing financial interests or personal relationships that could have appeared to influence the work reported in this paper.

Data availability

Data will be made available on request.

Acknowledgements

Sponsorship of this research project by the Conselho Nacional de Desenvolvimento Científico e Tecnológico - Brasil (CNPq), project number 150417/2021-7, and by the São Paulo State Foundation for Research (FAPESP), project numbers 2016/23649-0 and 2019/03340-3, is greatly appreciated. This study was also financed in part by the Coordenação de Aperfeiçoamento de Pessoal de Nível Superior - Brasil (CAPES) - Finance Code 001.

Appendix A. Stress and displacement functions for interface cracks

When n is odd, the stress functions $\Sigma_{ij}^n(\theta, s)$ and $Y_{ij}^n(\theta, s)$ in Eq. (1) can be written as follows:

$$\Sigma_{11}^n(\theta,s) = \frac{1}{\cosh \pi\varepsilon}\left\{-\left[\sinh\left(\varepsilon(\Pi_s-\theta)\right) - e^{-\varepsilon(\Pi_s-\theta)}\right]\cos\frac{n-2}{2}\theta - \frac{1}{2}e^{-\varepsilon(\Pi_s-\theta)}\sin\theta\left[(n-2)\sin\frac{n-4}{2}\theta - 2\varepsilon\cos\frac{n-4}{2}\theta\right]\right\}$$

$$\Sigma_{12}^n(\theta,s) = \frac{1}{\cosh \pi\varepsilon}\left\{\sinh\left(\varepsilon(\Pi_s-\theta)\right)\sin\frac{n-2}{2}\theta - \frac{1}{2}e^{-\varepsilon(\Pi_s-\theta)}\sin\theta\left[(n-2)\cos\frac{n-4}{2}\theta + 2\varepsilon\sin\frac{n-4}{2}\theta\right]\right\}$$

$$\Sigma_{22}^n(\theta,s) = \frac{1}{\cosh \pi\varepsilon}\left\{\left[\sinh\left(\varepsilon(\Pi_s-\theta)\right) + e^{-\varepsilon(\Pi_s-\theta)}\right]\cos\frac{n-2}{2}\theta + \frac{1}{2}e^{-\varepsilon(\Pi_s-\theta)}\sin\theta\left[(n-2)\sin\frac{n-4}{2}\theta - 2\varepsilon\cos\frac{n-4}{2}\theta\right]\right\}$$

$$Y_{11}^n(\theta,s) = \frac{1}{\cosh \pi\varepsilon}\left\{\left[\cosh\left(\varepsilon(\Pi_s-\theta)\right) + e^{-\varepsilon(\Pi_s-\theta)}\right]\sin\frac{n-2}{2}\theta + \frac{1}{2}e^{-\varepsilon(\Pi_s-\theta)}\sin\theta\left[(n-2)\cos\frac{n-4}{2}\theta + 2\varepsilon\sin\frac{n-4}{2}\theta\right]\right\}$$

$$Y_{12}^n(\theta,s) = \frac{1}{\cosh \pi\varepsilon}\left\{\cosh\left(\varepsilon(\Pi_s-\theta)\right)\cos\frac{n-2}{2}\theta - \frac{1}{2}e^{-\varepsilon(\Pi_s-\theta)}\sin\theta\left[(n-2)\sin\frac{n-4}{2}\theta - 2\varepsilon\cos\frac{n-4}{2}\theta\right]\right\}$$

$$Y_{22}^n(\theta,s) = \frac{1}{\cosh \pi\varepsilon}\left\{-\left[\cosh\left(\varepsilon(\Pi_s-\theta)\right) - e^{-\varepsilon(\Pi_s-\theta)}\right]\sin\frac{n-2}{2}\theta - \frac{1}{2}e^{-\varepsilon(\Pi_s-\theta)}\sin\theta\left[(n-2)\cos\frac{n-4}{2}\theta + 2\varepsilon\sin\frac{n-4}{2}\theta\right]\right\}$$

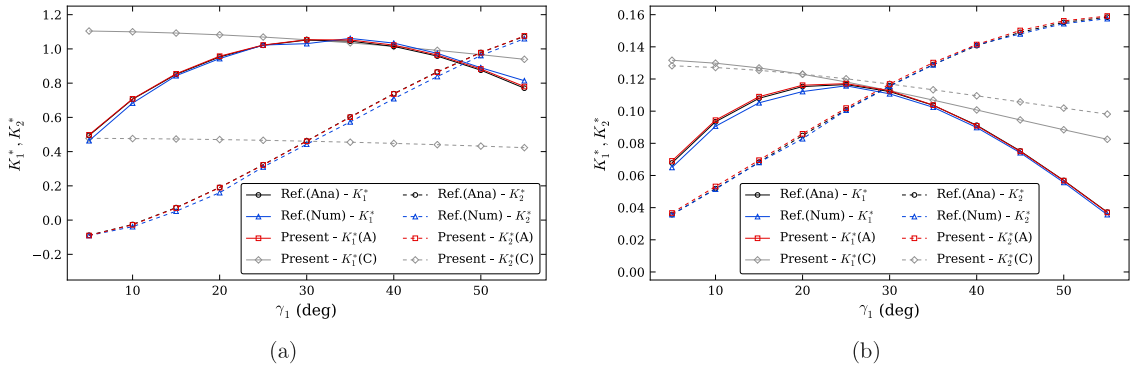

Fig. 22. Variation of the normalised SIFs with γ_1 considering the cases of (a) hard inclusion and (b) soft inclusion. The normalised SIF values are evaluated by $K_1^* + \mathrm{i}K_2^* = (K_1 + \mathrm{i}K_2) / \left(\sigma_0 \sqrt{2} R^{0.5+\mathrm{i}\varepsilon}\right)$. The solutions for tip A are compared with the semi-analytical (Ana) and numerical (Num) responses provided by Le et al. [69] (Section 4.6).

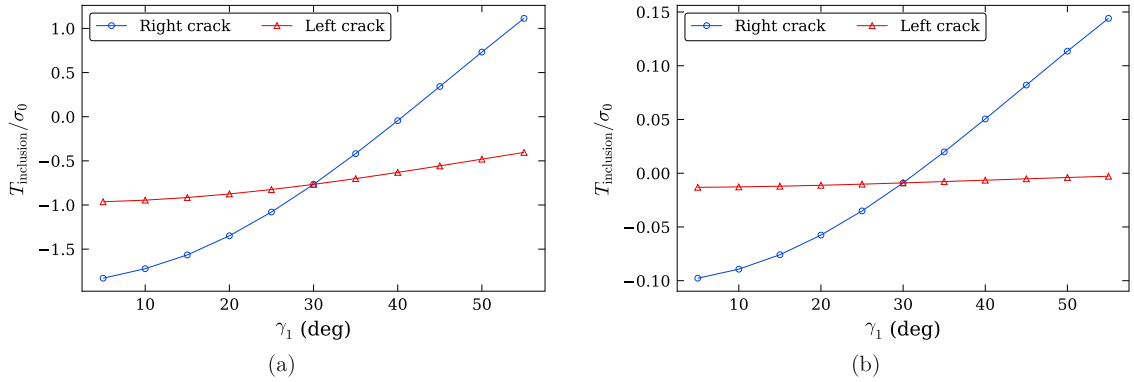

Fig. 23. Variation of the normalised T-stress in material 2 for right crack (tips A and B) and left crack (tips C and D) considering a (a) hard inclusion and a (b) soft inclusion (Section 4.6).

where $s = 1, 2$ indicates the upper and lower materials, respectively, and $\Pi_1 = \pi$ and $\Pi_2 = -\pi$: When n is even, the stress functions are obtained by:

$$\Sigma_{11}^n(\theta, s) = \frac{1}{1+\omega_s}\left\{4\cos\frac{n-2}{2}\theta - (n-2)\sin\theta\sin\frac{n-4}{2}\theta\right\}$$

$$\Sigma_{12}^n(\theta, s) = \frac{1}{1+\omega_s}\left\{-2\sin\frac{n-2}{2}\theta - (n-2)\sin\theta\cos\frac{n-4}{2}\theta\right\}$$

$$\Sigma_{22}^n(\theta, s) = \frac{1}{1+\omega_s}\left\{(n-2)\sin\theta\sin\frac{n-4}{2}\theta\right\}$$

$$Y_{11}^n(\theta, s) = \frac{1}{1+\omega_s}\left\{2\sin\frac{n-2}{2}\theta + (n-2)\sin\theta\cos\frac{n-4}{2}\theta\right\}$$

$$Y_{12}^n(\theta, s) = \frac{1}{1+\omega_s}\left\{-(n-2)\sin\theta\sin\frac{n-4}{2}\theta\right\}$$

$$Y_{22}^n(\theta, s) = \frac{1}{1+\omega_s}\left\{2\sin\frac{n-2}{2}\theta - (n-2)\sin\theta\cos\frac{n-4}{2}\theta\right\}$$

where $\omega_1 = \left[\left(\kappa_1+1\right)\mu_2\right] / \left[\left(\kappa_2+1\right)\mu_1\right]$ and $\omega_2 = \left[\left(\kappa_2+1\right)\mu_1\right] / \left[\left(\kappa_1+1\right)\mu_2\right]$. When n is odd, the displacement functions $\Delta_j^n(\theta, s)$ and $\Theta_j^n(\theta, s)$ in Eq. (3) are given by:

$$\begin{aligned}\Delta_1^n(\theta, s) = -\frac{1}{\mu_s\left(n^2+4\varepsilon^2\right)\cosh(\pi\varepsilon)}\Bigg\{&n\left[\sinh\left(\varepsilon(\Pi_s-\theta)\right) - \frac{\kappa_s-1}{2}e^{-\varepsilon(\Pi_s-\theta)}\right]\cos\frac{n\theta}{2} + \\ &+\frac{1}{2}\left(n^2+4\varepsilon^2\right)e^{-\varepsilon(\Pi_s-\theta)}\sin\theta\sin\frac{n-2}{2}\theta + 2\varepsilon\left[\cosh\left(\varepsilon(\Pi_s-\theta)\right)\right. \\ &\left.+\frac{\kappa_s-1}{2}e^{-\varepsilon(\Pi_s-\theta)}\right]\sin\frac{n\theta}{2}\Bigg\}\end{aligned}$$

$$\begin{aligned}\Delta_2^n(\theta, s) = \frac{1}{\mu_s\left(n^2+4\varepsilon^2\right)\cosh(\pi\varepsilon)}\Bigg\{&n\left[\cosh\left(\varepsilon(\Pi_s-\theta)\right) + \frac{\kappa_s-1}{2}e^{-\varepsilon(\Pi_s-\theta)}\right]\sin\frac{n\theta}{2} + \\ &-\frac{1}{2}\left(n^2+4\varepsilon^2\right)e^{-\varepsilon(\Pi_s-\theta)}\sin\theta\cos\frac{n-2}{2}\theta - 2\varepsilon\left[\sinh\left(\varepsilon(\Pi_s-\theta)\right)\right. \\ &\left.-\frac{\kappa_s-1}{2}e^{-\varepsilon(\Pi_s-\theta)}\right]\cos\frac{n\theta}{2}\Bigg\}\end{aligned}$$

$$\begin{aligned}\Theta_1^n(\theta, s) = \frac{1}{\mu_s\left(n^2+4\varepsilon^2\right)\cosh(\pi\varepsilon)}\Bigg\{&n\left[\cosh\left(\varepsilon(\Pi_s-\theta)\right) + \frac{\kappa_s-1}{2}e^{-\varepsilon(\Pi_s-\theta)}\right]\sin\frac{n\theta}{2} + \\ &+\frac{1}{2}\left(n^2+4\varepsilon^2\right)e^{-\varepsilon(\Pi_s-\theta)}\sin\theta\cos\frac{n-2}{2}\theta \\ &-2\varepsilon\left[\sinh\left(\varepsilon(\Pi_s-\theta)\right) - \frac{\kappa_s-1}{2}e^{-\varepsilon(\Pi_s-\theta)}\right]\cos\frac{n\theta}{2}\Bigg\}\end{aligned}$$

$$\begin{aligned}\Theta_2^n(\theta, s) = \frac{1}{\mu_s\left(n^2+4\varepsilon^2\right)\cosh(\pi\varepsilon)}\Bigg\{&n\left[\sinh\left(\varepsilon(\Pi_s-\theta)\right) - \frac{\kappa_s-1}{2}e^{-\varepsilon(\Pi_s-\theta)}\right]\cos\frac{n\theta}{2} + \\ &-\frac{1}{2}\left(n^2+4\varepsilon^2\right)e^{-\varepsilon(\Pi_s-\theta)}\sin\theta\sin\frac{n-2}{2}\theta \\ &+2\varepsilon\left[\cosh\left(\varepsilon(\Pi_s-\theta)\right) + \frac{\kappa_s-1}{2}e^{-\varepsilon(\Pi_s-\theta)}\right]\sin\frac{n\theta}{2}\Bigg\}\end{aligned}$$

For n even, the displacement functions are expressed by:

$$\Delta_1^n(\theta, s) = \frac{1}{\mu_s n\left(1+\omega_s\right)}\left[\left(\kappa_s+1\right)\cos\frac{n\theta}{2} - n\sin\theta\sin\frac{n-2}{2}\theta\right]$$

$$\Delta_2^n(\theta, s) = \frac{1}{\mu_s n\left(1+\omega_s\right)}\left[\left(\kappa_s-1\right)\sin\frac{n\theta}{2} - n\sin\theta\cos\frac{n-2}{2}\theta\right]$$

$$\Theta_1^n(\theta, s) = \frac{1}{\mu_s n\left(1+\omega_s\right)}\left[\left(\kappa_s-1\right)\sin\frac{n\theta}{2} + n\sin\theta\cos\frac{n-2}{2}\theta\right]$$

$$\Theta_2^n(\theta, s) = \frac{1}{\mu_s n\left(1+\omega_s\right)}\left[-\left(\kappa_s+1\right)\cos\frac{n\theta}{2} - n\sin\theta\sin\frac{n-2}{2}\theta\right]$$

Appendix B. Regularisation of integrals containing traction enrichment for tip element

The integral kernels containing only non-singular terms can be computed using Gauss–Legendre quadrature, with the accuracy of the

integration depending on the number of Gauss points used in the quadrature. However, the integral over the tip elements on the interface, which contains the traction enrichment in Eq. (36), must be firstly regularised since the enrichment function is singular at $\rho = 0$. Without loss of generality, considering a tip element at the upper material, the integral is written as:

$$\tilde{U}^{e\lambda I}_{iM} = \int_{-1}^{1} U^{*}_{ij}(\mathbf{x}', \mathbf{x}(\hat{\xi}))T^{\lambda}_{jk}\varpi^{I}_{kM}(\mathbf{x}^{\lambda}, \mathbf{x}(\hat{\xi}))J^{e}(\hat{\xi})d\hat{\xi} \tag{B.1}$$

To remove the singularity at the crack tip ($\hat{\xi} = -1$), a transformation of the parent space coordinate in terms of a new variable $\eta \in [-1, 1]$ can be written as follows:

$$\hat{\xi}(\eta) = \frac{1}{2}\left(\eta^2 + 2\eta - 1\right) \tag{B.2}$$

Then, the integral kernel in Eq. (B.1) can be rewritten as:

$$\tilde{U}^{e\lambda I}_{iM} = \int_{-1}^{1} U^{*}_{ij}\mathbf{x}', \mathbf{x}(\eta)R^{\lambda}_{jk}\varpi^{I}_{kM}(\mathbf{x}^{\lambda}, \mathbf{x}(\eta))J^{e}(\eta)\,(\eta + 1)\,d\eta \tag{B.3}$$

The above expression can be computed following the steps below:

1. Take an integration point to be η
2. Compute the transformed coordinate $\hat{\xi}$ with Eq. (B.2)
3. Define the coordinates $\mathbf{x}(\hat{\xi})$, the Jacobian $J^{e}(\hat{\xi})$ and the fundamental solution $U^{*}_{ij}(\mathbf{x}', \mathbf{x}(\hat{\xi}))$ at the coordinate $\hat{\xi}$
4. Compute the distance from the tip $\rho := \left\|\mathbf{x}(\hat{\xi}) - \mathbf{x}^{\lambda}\right\|$ and determine the enrichment function $\varpi^{I}_{kM}(\mathbf{x}^{\lambda}, \mathbf{x}(\hat{\xi}))$
5. Evaluate the integrand of Eq. (B.3) and multiply it by the weight corresponding to the integration point. Increment the value of the integral
6. Take the next integration point η and return to 2

If the tip element contains the source point, Telles' transformation [70] can be used to regularise the weakly singular integrand that appears due to the singularity of the fundamental solution U^{*}_{ij}. Note that since discontinuous NURBS are adopted to model the crack and interface surfaces, there is no collocation point at the crack tip ($\rho = 0$). Therefore, the singularity arising from U^{*}_{ij} when the tip element contains the source point $\mathbf{x}'$ does not occur at the same singular point of ϖ^{I}_{kM}.

References

[1] M. Williams, The stresses around a fault or crack in dissimilar media, Bull. Seismol. Soc. Am. 49 (2) (1959) 199–204.

[2] A. England, A crack between dissimilar media, J. Appl. Mech 32 (2) (1965) 400–402, http://dx.doi.org/10.1115/1.3625813.

[3] F. Erdogan, Stress distribution in bonded dissimilar materials with cracks, J. Appl. Mech. 32 (2) (1965) 403–410, http://dx.doi.org/10.1115/1.3625814.

[4] J.R. Rice, G.C. Sih, Plane problems of cracks in dissimilar media, J. Appl. Mech. 32 (2) (1965) 418–423, http://dx.doi.org/10.1115/1.3625816.

[5] L. Banks-Sills, Interface Fracture and Delaminations in Composite Materials, Springer, 2018.

[6] M. Comninou, An overview of interface cracks, Eng. Fract. Mech. 37 (1) (1990) 197–208, http://dx.doi.org/10.1016/0013-7944(90)90343-f.

[7] J.W. Hutchinson, M.E. Mear, J.R. Rice, Crack paralleling an interface between dissimilar materials, J. Appl. Mech. 54 (4) (1987) 828–832, http://dx.doi.org/10.1115/1.3173124.

[8] J. Rice, Elastic fracture mechanics concepts for interfacial cracks, J. Appl. Mech. 55 (1) (1988) 98–103, http://dx.doi.org/10.1115/1.3173668.

[9] J.R. Rice, Z. Suo, J.-S. Wang, Mechanics and thermodynamics of brittle interfacial failure in bimaterial systems, Acta-Scr. Metall. Proc. Ser. 4 (1990) 269–294, http://dx.doi.org/10.1016/B978-0-08-040505-6.50036-2.

[10] J. Hutchinson, Z. Suo, Mixed mode cracking in layered materials, in: Advances in Applied Mechanics, Elsevier, 1991, pp. 63–191, http://dx.doi.org/10.1016/s0065-2156(08)70164-9.

[11] M. Gupta, R. Alderliesten, R. Benedictus, A review of T-stress and its effects in fracture mechanics, Eng. Fract. Mech. 134 (2015) 218–241.

[12] B. Cotterell, J. Rice, Slightly curved or kinked cracks, Int. J. Fract. 16 (2) (1980) 155–169, http://dx.doi.org/10.1007/bf00012619.

[13] M.-Y. He, A. Bartlett, A.G. Evans, J.W. Hutchinson, Kinking of a crack out of an interface: Role of in-plane stress, J. Am. Ceram. Soc. 74 (4) (1991) 767–771, http://dx.doi.org/10.1111/j.1151-2916.1991.tb06922.x.

[14] M. Mirsayar, On fracture of kinked interface cracks – The role of T-stress, Mater. Des. 61 (2014) 117–123.

[15] S.G. Larsson, A.J. Carlsson, Influence of non-singular stress terms and specimen geometry on small-scale yielding at crack tips in elastic-plastic materials, J. Mech. Phys. Solids 21 (4) (1973) 263–277, http://dx.doi.org/10.1016/0022-5096(73)90024-0.

[16] Z. Suo, J.W. Hutchinson, Interface crack between two elastic layers, Int. J. Fract. 43 (1) (1990) 1–18, http://dx.doi.org/10.1007/bf00018123.

[17] D.-H. Chen, S. Nakamichi, Stress intensity factors for an interface crack along an elliptical inclusion, Int. J. Fract. 82 (2) (1996) 131–152, http://dx.doi.org/10.1007/bf00034660.

[18] J.-H. Kim, J.J. Vlassak, T-stress of a bi-material strip under generalized edge loads, Int. J. Fract. 142 (3–4) (2007) 315–322, http://dx.doi.org/10.1007/s10704-006-9033-6.

[19] J. Yau, S. Wang, An analysis of interface cracks between dissimilar isotropic materials using conservation integrals in elasticity, Eng. Fract. Mech. 20 (3) (1984) 423–432, http://dx.doi.org/10.1016/0013-7944(84)90048-1.

[20] A. Kfouri, Some evaluations of the elastic T-term using Eshelby's method, Int. J. Fract. 30 (4) (1986) 301–315, http://dx.doi.org/10.1007/bf00019710.

[21] P.P.L. Matos, R.M. McMeeking, P.G. Charalambides, M.D. Drory, A method for calculating stress intensities in bimaterial fracture, Int. J. Fract. 40 (4) (1989) 235–254, http://dx.doi.org/10.1007/bf00963659.

[22] K.Y. Lee, H.J. Choi, Boundary element analysis of stress intensity factors for bimaterial interface cracks, Eng. Fract. Mech. 29 (4) (1988) 461–472, http://dx.doi.org/10.1016/0013-7944(88)90033-1.

[23] Y. Ryoji, C. Sang-Bong, Efficient boundary element analysis of stress intensity factors for interface cracks in dissimilar materials, Eng. Fract. Mech. 34 (1) (1989) 179–188, http://dx.doi.org/10.1016/0013-7944(89)90251-8.

[24] N. Miyazaki, T. Ikeda, T. Soda, T. Munakata, Stress intensity factor analysis of interface crack using boundary element method—Application of contour-integral method, Eng. Fract. Mech. 45 (5) (1993) 599–610, http://dx.doi.org/10.1016/0013-7944(93)90266-u.

[25] J. Sladek, V. Sladek, Evaluations of the T-stress for interface cracks by the boundary element method, Eng. Fract. Mech. 56 (6) (1997) 813–825, http://dx.doi.org/10.1016/s0013-7944(96)00131-2.

[26] T. Nagashima, Y. Omoto, S. Tani, Stress intensity factor analysis of interface cracks using X-FEM, Internat. J. Numer. Methods Engrg. 56 (8) (2003) 1151–1173.

[27] N. Sukumar, Z.Y. Huang, J.-H. Prévost, Z. Suo, Partition of unity enrichment for bimaterial interface cracks, Internat. J. Numer. Methods Engrg. 59 (8) (2004) 1075–1102, http://dx.doi.org/10.1002/nme.902.

[28] H. Yu, L. Wu, L. Guo, Q. He, S. Du, Interaction integral method for the interfacial fracture problems of two nonhomogeneous materials, Mech. Mater. 42 (4) (2010) 435–450, http://dx.doi.org/10.1016/j.mechmat.2010.01.001.

[29] H. Yu, L. Wu, H. Li, T-stress evaluations of an interface crack in the materials with complex interfaces, Int. J. Fract. 177 (1) (2012) 25–37, http://dx.doi.org/10.1007/s10704-012-9747-6.

[30] J. Melenk, I. Babuska, The partition of unity finite element method: Basic theory and applications, Comput. Methods Appl. Mech. Engrg. 139 (1–4) (1996) 289–314, http://dx.doi.org/10.1016/s0045-7825(96)01087-0.

[31] I. Babuska, J.M. Melenk, The partition of unity method, Internat. J. Numer. Methods Engrg. 40 (4) (1997) 727–758, http://dx.doi.org/10.1002/(sici)1097-0207(19970228)40:4<727::aid-nme86>3.0.co;2-n.

[32] C. Tan, Y. Gao, Treatment of bimaterial interface crack problems using the boundary element method, Eng. Fract. Mech. 36 (6) (1990) 919–932, http://dx.doi.org/10.1016/0013-7944(90)90268-l.

[33] Y. Gao, C. Tan, Determination of characterizing parameters for bimaterial interface cracks using the boundary element method, Eng. Fract. Mech. 41 (5) (1992) 779–784, http://dx.doi.org/10.1016/0013-7944(92)90160-g.

[34] Y.J. Liu, N. Xu, Modeling of interface cracks in fiber-reinforced composites with the presence of interphases using the boundary element method, Mech. Mater. 32 (12) (2000) 769–783, http://dx.doi.org/10.1016/s0167-6636(00)00045-4.

[35] Y. Gu, C. Zhang, Novel special crack-tip elements for interface crack analysis by an efficient boundary element method, Eng. Fract. Mech. 239 (2020) 107302, http://dx.doi.org/10.1016/j.engfracmech.2020.107302.

[36] A.R. Ingraffea, C. Manu, Stress-intensity factor computation in three dimensions with quarter-point elements, Internat. J. Numer. Methods Engrg. 15 (10) (1980) 1427–1445, http://dx.doi.org/10.1002/nme.1620151002.

[37] L. Harrop, The optimum size of quarter-point crack tip elements, Internat. J. Numer. Methods Engrg. 18 (7) (1982) 1101–1103, http://dx.doi.org/10.1002/nme.1620180713.

[38] J. Martínez, J. Domínguez, On the use of quarter-point boundary elements for stress intensity factor computations, Internat. J. Numer. Methods Engrg. 20 (10) (1984) 1941–1950, http://dx.doi.org/10.1002/nme.1620201013.

[39] N.A.B. Yehia, M.S. Shephard, On the effect of quarter-point element size on fracture criteria, Internat. J. Numer. Methods Engrg. 21 (10) (1985) 1911–1924, http://dx.doi.org/10.1002/nme.1620211014.

[40] J. Rice, A path independent integral and the approximate analysis of strain concentration by notches and cracks, J. Appl. Mech. 35 (2) (1968) 379, http://dx.doi.org/10.1115/1.3601206.

[41] V. González-Albuixech, E. Giner, J. Tarancón, F. Fuenmayor, A. Gravouil, Convergence of domain integrals for stress intensity factor extraction in 2-D curved cracks problems with the extended finite element method, Internat. J. Numer. Methods Engrg. 94 (8) (2013) 740–757, http://dx.doi.org/10.1002/nme.4478.
[42] M.M. Chiaramonte, Y. Shen, L.M. Keer, A.J. Lew, Computing stress intensity factors for curvilinear cracks, Internat. J. Numer. Methods Engrg. 104 (4) (2015) 260–296, http://dx.doi.org/10.1002/nme.4938.
[43] X.Y. Liu, Q.Z. Xiao, B.L. Karihaloo, XFEM for direct evaluation of mixed mode SIFs in homogeneous and bi-materials, Internat. J. Numer. Methods Engrg. 59 (8) (2004) 1103–1118, http://dx.doi.org/10.1002/nme.906.
[44] Y. Wang, C. Cerigato, H. Waisman, E. Benvenuti, XFEM with high-order material-dependent enrichment functions for stress intensity factors calculation of interface cracks using Irwin's crack closure integral, Eng. Fract. Mech. 178 (2017) 148–168, http://dx.doi.org/10.1016/j.engfracmech.2017.04.021.
[45] C. Song, Evaluation of power-logarithmic singularities, T-stresses and higher order terms of in-plane singular stress fields at cracks and multi-material corners, Eng. Fract. Mech. 72 (10) (2005) 1498–1530, http://dx.doi.org/10.1016/j.engfracmech.2004.11.002.
[46] S. Natarajan, C. Song, S. Belouettar, Numerical evaluation of stress intensity factors and T-stress for interfacial cracks and cracks terminating at the interface without asymptotic enrichment, Comput. Methods Appl. Mech. Engrg. 279 (2014) 86–112, http://dx.doi.org/10.1016/j.cma.2014.06.024.
[47] R. Simpson, J. Trevelyan, A partition of unity enriched dual boundary element method for accurate computations in fracture mechanics, Comput. Methods Appl. Mech. Engrg. 200 (1–4) (2011) 1–10, http://dx.doi.org/10.1016/j.cma.2010.06.015.
[48] I. Alatawi, J. Trevelyan, A direct evaluation of stress intensity factors using the extended dual boundary element method, Eng. Anal. Bound. Elem. 52 (2015) 56–63, http://dx.doi.org/10.1016/j.enganabound.2014.11.022.
[49] G. Hattori, I.A. Alatawi, J. Trevelyan, An extended boundary element method formulation for the direct calculation of the stress intensity factors in fully anisotropic materials, Internat. J. Numer. Methods Engrg. 109 (7) (2016) 965–981, http://dx.doi.org/10.1002/nme.5311.
[50] H. Andrade, E. Leonel, An enriched dual boundary element method formulation for linear elastic crack propagation, Eng. Anal. Bound. Elem. 121 (2020) 158–179, http://dx.doi.org/10.1016/j.enganabound.2020.09.007.
[51] X. Peng, E. Atroshchenko, P. Kerfriden, S. Bordas, Isogeometric boundary element methods for three dimensional static fracture and fatigue crack growth, Comput. Methods Appl. Mech. Engrg. 316 (2017) 151–185, http://dx.doi.org/10.1016/j.cma.2016.05.038.
[52] H. Andrade, J. Trevelyan, E. Leonel, A NURBS-discontinuous and enriched isogeometric boundary element formulation for two-dimensional fatigue crack growth, Eng. Anal. Bound. Elem. 134 (2022) 259–281, http://dx.doi.org/10.1016/j.enganabound.2021.09.019.
[53] X. Deng, General crack-tip fields for stationary and steadily growing interface cracks in anisotropic bimaterials, J. Appl. Mech. 60 (1) (1993) 183–189, http://dx.doi.org/10.1115/1.2900743.
[54] P. Banerjee, Integral equation methods for analysis of piece-wise non-homogeneous three-dimensional elastic solids of arbitrary shape, Int. J. Mech. Sci. 18 (6) (1976) 293–303, http://dx.doi.org/10.1016/0020-7403(76)90031-x.
[55] G.E. Blandford, A.R. Ingraffea, J.A. Liggett, Two-dimensional stress intensity factor computations using the boundary element method, Internat. J. Numer. Methods Engrg. 17 (3) (1981) 387–404, http://dx.doi.org/10.1002/nme.1620170308.
[56] R. Simpson, S. Bordas, J. Trevelyan, T. Rabczuk, A two-dimensional isogeometric boundary element method for elastostatic analysis, Comput. Methods Appl. Mech. Engrg. 209–212 (2012) 87–100, http://dx.doi.org/10.1016/j.cma.2011.08.008.
[57] R. Simpson, S. Bordas, H. Lian, J. Trevelyan, An isogeometric boundary element method for elastostatic analysis: 2D implementation aspects, Computers & Structures 118 (2013) 2–12, http://dx.doi.org/10.1016/j.compstruc.2012.12.021.
[58] M.G. Cox, The numerical evaluation of B-splines, IMA J. Appl. Math. 10 (2) (1972) 134–149, http://dx.doi.org/10.1093/imamat/10.2.134.
[59] C. De Boor, On calculating with B-splines, J. Approx. Theory 6 (1) (1972) 50–62, http://dx.doi.org/10.1016/0021-9045(72)90080-9.
[60] Y. Wang, H. Waisman, I. Harari, Direct evaluation of stress intensity factors for curved cracks using Irwin's integral and XFEM with high-order enrichment functions, Internat. J. Numer. Methods Engrg. 112 (7) (2017) 629–654, http://dx.doi.org/10.1002/nme.5517.
[61] T. Greville, Numerical procedures for interpolation by spline functions, J. Soc. Ind. Appl. Math. Ser. B Numer. Anal. 1 (1) (1964) 53–68, http://dx.doi.org/10.1137/0701005.
[62] R.W. Johnson, Higher order B-spline collocation at the Greville abscissae, Appl. Numer. Math. 52 (1) (2005) 63–75, http://dx.doi.org/10.1016/j.apnum.2004.04.002.
[63] L. Piegl, W. Tiller, The NURBS Book, Springer Berlin Heidelberg, 1995, http://dx.doi.org/10.1007/978-3-642-97385-7.
[64] A. Perlman, G. Sih, Elastostatic problems of curvilinear cracks in bonded dissimilar materials, Internat. J. Engrg. Sci. 5 (11) (1967) 845–867, http://dx.doi.org/10.1016/0020-7225(67)90009-2.
[65] Y. Chen, Closed form solutions of T-stress in plane elasticity crack problems, Int. J. Solids Struct. 37 (11) (2000) 1629–1637, http://dx.doi.org/10.1016/s0020-7683(98)00312-6.
[66] N. Muthu, S. Maiti, B. Falzon, W. Yan, Crack propagation in non-homogenous materials: Evaluation of mixed-mode SIFs, T-stress and kinking angle using a variant of EFG method, Eng. Anal. Bound. Elem. 72 (2016) 11–26, http://dx.doi.org/10.1016/j.enganabound.2016.07.017.
[67] L. Wu, H. Yu, L. Guo, Q. He, S. Du, Investigation of stress intensity factors for an interface crack in multi-interface materials using an interaction integral method, J. Appl. Mech. 78 (6) (2011) http://dx.doi.org/10.1115/1.4003906.
[68] A. Portela, M.H. Aliabadi, D.P. Rooke, The dual boundary element method: Effective implementation for crack problems, Internat. J. Numer. Methods Engrg. 33 (6) (1992) 1269–1287, http://dx.doi.org/10.1002/nme.1620330611.
[69] V. Le, S. Brisard, A. Pouya, Debonding of a circular inclusion: Asymmetric propagation of a pair of cracks, Int. J. Solids Struct. 167 (2019) 71–78, http://dx.doi.org/10.1016/j.ijsolstr.2019.03.004.
[70] J. Telles, A self-adaptive co-ordinate transformation for efficient numerical evaluation of general boundary element integrals, Internat. J. Numer. Methods Engrg. 24 (5) (1987) 959–973, http://dx.doi.org/10.1002/nme.1620240509.